

Structure–Activity Relationship in a Purine-Scaffold Compound Series with Selectivity for the Endoplasmic Reticulum Hsp90 Paralog Grp94

Hardik J. Patel,[†] Pallav D. Patel,^{†,‡} Stefan O. Ochiana,[†] Pengrong Yan,[†] Weilin Sun,[†] Maulik R. Patel,[†] Smit K. Shah,[†] Elisa Tramentozzi,[§] James Brooks,^{||} Alexander Bolaender,[†] Liza Shrestha,[†] Ralph Stephani,[‡] Paola Finotti,[§] Cynthia Leifer,^{||} Zihai Li,[⊥] Daniel T. Gewirth,[#] Tony Taldone,^{*,†} and Gabriela Chiosis^{*,†}

[†]Molecular Pharmacology and Chemistry Program, Sloan-Kettering Institute, New York, New York 10021, United States

[‡]Department of Pharmaceutical Sciences, College of Pharmacy and Allied Health Professions, St. John's University, Jamaica, New York 11439, United States

[§]Department of Pharmacology and Anesthesiology, University of Padua, Largo E. Meneghetti 2, 35131, Padua, Italy

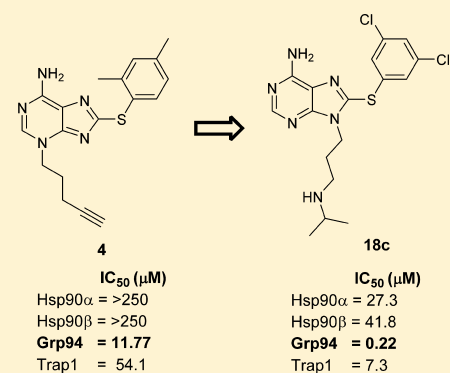
^{||}Department of Microbiology and Immunology, Cornell University, Ithaca, New York 14850, United States

[⊥]Department of Microbiology and Immunology, Medical University of South Carolina, Charleston, South Carolina United States

[#]Hauptman-Woodward Medical Research Institute, Buffalo, New York 14203, United States

S Supporting Information

ABSTRACT: Grp94 is involved in the regulation of a restricted number of proteins and represents a potential target in a host of diseases, including cancer, septic shock, autoimmune diseases, chronic inflammatory conditions, diabetes, coronary thrombosis, and stroke. We have recently identified a novel allosteric pocket located in the Grp94 N-terminal binding site that can be used to design ligands with a 2-log selectivity over the other Hsp90 paralogs. Here we perform extensive SAR investigations in this ligand series and rationalize the affinity and paralog selectivity of choice derivatives by molecular modeling. We then use this to design **18c**, a derivative with good potency for Grp94 ($IC_{50} = 0.22 \mu M$) and selectivity over other paralogs (>100- and 33-fold for Hsp90 α/β and Trap-1, respectively). The paralog selectivity and target-mediated activity of **18c** was confirmed in cells through several functional readouts. Compound **18c** was also inert when tested against a large panel of kinases. We show that **18c** has biological activity in several cellular models of inflammation and cancer and also present here for the first time the in vivo profile of a Grp94 inhibitor.



INTRODUCTION

Glucose-regulated protein 94 (Grp94),¹ also known as gp96, ERp99, and endoplasmic reticulum (ER) paralog of the Hsp90 family of molecular chaperones. In addition to Grp94, the members of this family include the cytosolic Hsp90 α , Hsp90 β , and the mitochondrial tumor necrosis factor receptor-associated protein-1 (Trap-1). While highly homologous, with over 50% sequence identity in their N-terminal regulatory domains and analogous ligand binding cavities, it is now recognized that each paralog has a unique biochemical role and is responsible for chaperoning a distinct set of client proteins.^{2–4}

Sustained medical interest in cytoplasmic Hsp90 has come from the discovery that these chaperones play important roles in maintaining the functional conformation of a large number of malignancy- and neurodegeneration-driving proteins, such as kinases, transcription factors, and antiapoptotic proteins.³ In addition, Trap-1 along with Hsp90 maintains mitochondrial integrity by protecting against oxidative stress and apoptosis.^{5,6}

Grp94 has recently also emerged as an attractive target in cancer. Clinically, Grp94 expression correlates with advanced stage and poor survival in a variety of cancers and is closely linked to cancer growth and metastasis in melanoma, breast cancer, ovarian cancer, multiple myeloma, lung cancer, and inflammation-associated colon cancer.^{2,7,8} It also is linked to tumor resistance, where Grp94 expression in tumors decreases sensitivity to X-rays and its suppression sensitizes cells to chemotherapy.^{2,7} While the exact role for Grp94 in cancer remains elusive, its function as an essential chaperone for TLRs, integrins, GARP, and Wnt coreceptor LRP5/6 is suggestive of a potential link between Grp94 and aberrant signaling via these receptors. Evidence also points to Grp94's involvement at the ER level in regulating a number of tyrosine kinases, such as EGFR and HER2, and in regulating the secretion of IGF-I and IGF-II.^{2,7,8} Finally, the recent discovery that tumor-specific

Received: February 3, 2015

Published: April 22, 2015

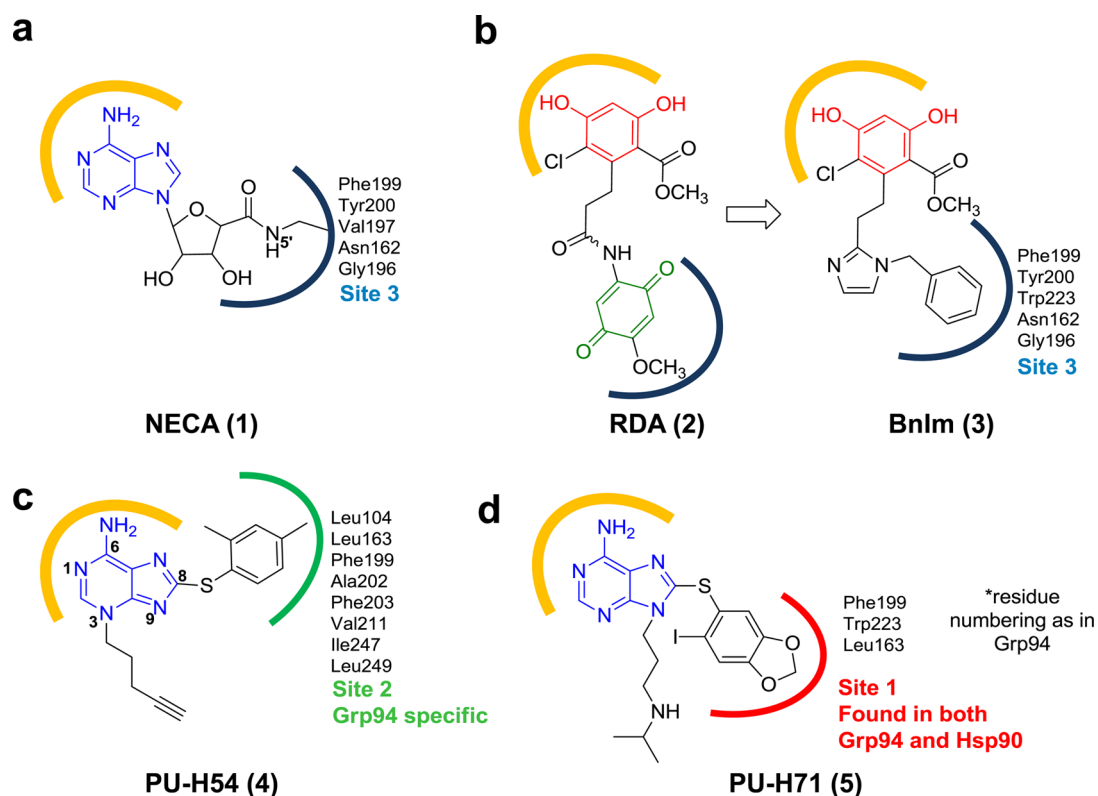


Figure 1. A schematic depiction of (a) 1, (b) 2 and 3, and the amino acids present in site 3 of Grp94 (adapted from refs 11, 14, and 17); (c) 4 and the amino acids present in the allosteric site 2 of Grp94 (adapted from ref 10); and (d) 5 (pan-Hsp90 inhibitor) and the amino acids found in site 1 of Grp94. The conserved adenine binding pocket is shown in orange. The adenine moiety is shown in blue, the quinone in green, and the resorcinol core in red.

translocation of Grp94 to the plasma membrane regulates the altered expression and function of membrane-associated cancer proteins, such as HER2, and its role in sustaining the transforming ability of these proteins point to a third avenue for Grp94's involvement in cancer.^{9,10}

Because Grp94 is involved in the regulation of a restricted number of proteins involved in channeling immune and inflammatory signals, it has been proposed that, in addition to cancer, numerous other diseases, including septic shock, autoimmune diseases, chronic inflammatory conditions, diabetes, coronary thrombosis, and stroke, would benefit from targeting Grp94 with small-molecule inhibitors.^{2,7,8} Most important from a therapeutic perspective, the chaperoning activity of Grp94 is ATPase-dependent and uncoupled from its ability to bind peptides, a role of Grp94 linked to the immunogenic activity of Grp94/peptide complexes. Together, these findings highlight a potential therapeutic role for small molecules that bind selectively to Grp94 and inhibit its chaperoning function.

The rational development of selective Grp94 inhibitors has been challenging due to a high degree of sequence conservation in the ATP binding pockets of the four Hsp90 paralogs (Figure S1, Supporting Information). Nevertheless, screening identified 5'-N-ethylcarboxamidoadenosine (NECA, 1) (Figure 1a) as a high-affinity ligand with selectivity for Grp94.^{11,12} NECA has sub-micromolar ($K_d = 200$ nM) binding affinity for Grp94, while having no affinity for cytoplasmic Hsp90s.^{11,12} This serendipitous discovery was initially puzzling given the fact that the amino acids surrounding the adenine binding cavity in Grp94 and Hsp90 are almost entirely conserved. However, further examination revealed that Grp94 adopts a distinct

conformation due to a 5-amino acid (QEDGQ) insertion in its helix 1,4,5-subdomain. This conformation exposes a cavity adjacent to the adenine binding pocket that accommodates the 5'-N-ethylcarboxamido moiety of NECA (depicted as site 3 in Figure 1a). In yeast Hsp90, the analogous cavity is blocked by the backbone carbonyl oxygen of Gly121, which suggests that this is the origin of NECA binding selectivity.¹¹ This cavity is not utilized by bound nucleotides, as modeling shows that both α - and β -phosphates of ADP experience severe steric clashes with the carbonyl oxygen of Gly196 in Grp94. Instead, binding of nucleotides induces large conformational changes in helices 1,4,5 in Grp94 that enlarge the ATP binding cavity and allow for nucleotide binding.¹³ Unfortunately, attempts to develop more potent analogs of NECA have been unsuccessful.¹⁴ While NECA has served an important role in substantiating the feasibility of developing Grp94-selective inhibitors, its use as a probe to investigate Grp94 function suffers from its potent agonist activity against several cellular adenosine receptors.¹⁵

Radamide (RDA, 2) (Figure 1b) is a chimeric molecule composed of elements from both geldanamycin and radicicol and is the second ligand reported to bind into the small binding pocket unique to Grp94 (site 3, Figure 1b).^{14,16} X-ray crystal structures of RDA bound to the N-terminal domain of either canine Grp94 (PDB ID: 2GFD) or yeast Hsp90 (PDB ID: 2FXS) reveal that it adopts distinct poses when bound to either of the two paralogs. While the resorcinol moiety binds similarly into the adenine binding cavity of each paralog, the quinone ring is oriented differently. In Grp94, the quinone ring is capable of binding in two distinct poses, one of which orients the quinone ring into the same binding pocket that accommodates the 5'-N-ethylcarboxamido moiety of NECA

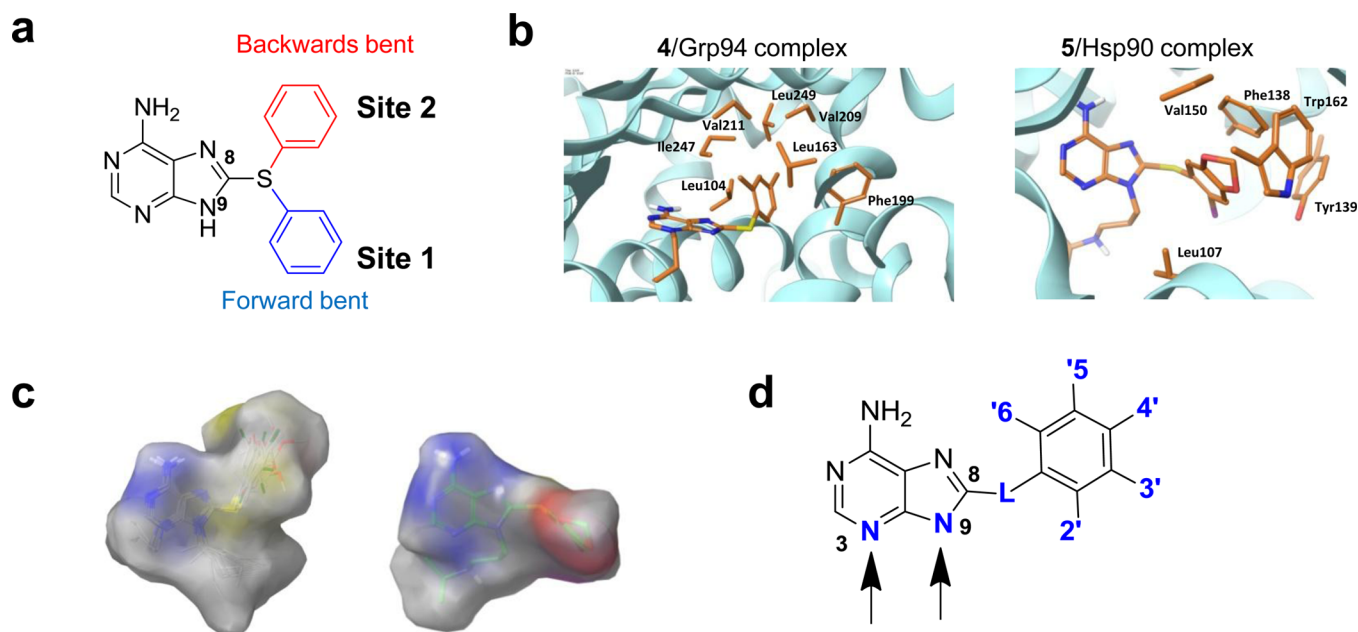


Figure 2. (a) Schematic depiction of the pose adapted by ligands when accessing the two binding sites, site 2 being specific to Grp94 and site 1 being common to Grp94 and Hsp90. (b) Pose adapted by 4 when bound to Grp94 showing the hydrophobic stabilization of the 8-aryl group with the hydrophobic residues of site 2 and the pose adapted by 5 when bound to Hsp90. (c) Surface area of the Grp94-selective ligands reported in ref 10 (left) and of the pan-Hsp90 ligand 5 (right) (surface area was generated with Macromodel/Molecular Surface). (d) Proposed modification sites on the purine scaffold performed to understand the structure–activity relationship in this series (as shown in blue).

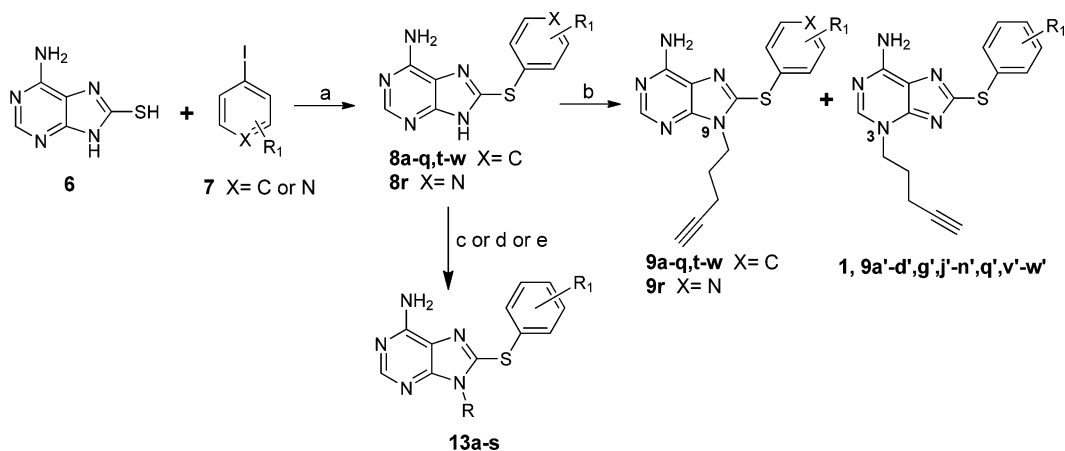
that is unique to Grp94 (site 3, Figure 1a,b) and another that orients it toward the solvent. In Hsp90, the quinone ring is blocked from binding into the analogous site 3 pocket by Lys98 and instead adopts the solvent-oriented pose. Though RDA interacts with the two paralogs in a very distinct manner and is capable of binding into the unique pocket of Grp94, it is not very selective for Grp94 ($K_d = 0.52 \mu\text{M}$) over Hsp90 ($K_d = 0.87 \mu\text{M}$).¹⁴ Since the quinone moiety of RDA is joined to the resorcinol via an amide linkage, upon binding to Grp94 it can adopt either the *cis*-amide conformation to bind into the hydrophobic pocket unique to Grp94 or the *trans*-amide conformation to orient toward the outside of the pocket, similar to that adopted when bound to Hsp90. Realizing that this conformational flexibility was the likely cause for the lack of selectivity of RDA, Duerfeldt et al.¹⁷ rationalized that compounds of greater selectivity for Grp94 might be obtained by restricting the orientation of RDA to the *cis*-conformation. Furthermore, observing that the pocket was lined by Phe199, Tyr200, and Trp223 (Figure 1b) made them seek to enhance its hydrophobicity and potential for π – π interactions. Utilizing imidazole as a *cis*-bioisostere to direct a more hydrophobic benzyl moiety into the pocket provided among others compound BnIm (3, Figure 1b). While BnIm was shown to have an $\text{IC}_{50} = 1.15 \mu\text{M}$ for Grp94 in a fluorescent polarization (FP) competitive binding assay using FITC-GM as a probe,¹⁸ similar competition experiments for each of the other isoforms were not performed.

Recently, we have reported the discovery of a novel, therapeutically viable allosteric pocket in Grp94 (i.e., site 2, Figure 1c) whose occupancy led to the inhibition of Grp94's chaperoning activity.¹⁰ The newly discovered site 2, which is composed of an almost completely hydrophobic cleft lined by Leu104, Leu163, Phe199, Ala202, Phe203, Val211, Ile247, and Leu249, is distinct from the pocket previously reported for 1 (i.e., site 3, Figure 1a)¹¹ and the resorcinolic *N*-benzylimidazole

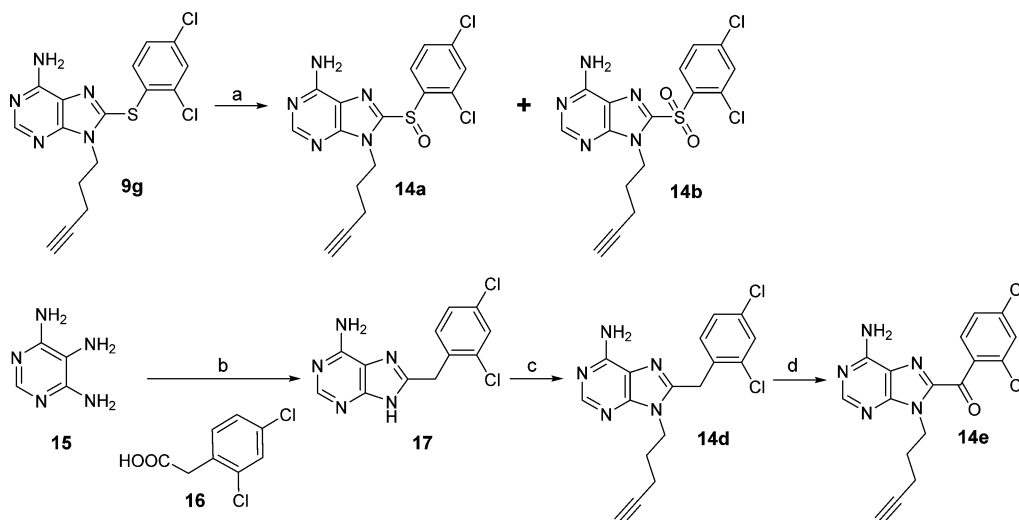
3 (i.e., site 3, Figure 1b).¹⁷ In addition to its distinct spatial orientation, site 2 is significantly more hydrophobic compared to site 1. Small-molecule purine-based ligands that utilize this novel pocket exhibited greater than 100-fold preference for Grp94 over Hsp90 α/β and a 10–100-fold preference over Trap-1.¹⁰ The crystal structure of Grp94 in complex with the selective ligand 4 (Figure 1c) showed that while the purine moiety of 4 occupied the site filled by the adenine ring of ATP and of the pan-Hsp90 inhibitor 5 (PU-H71; Figure 1d), the 8-aryl group of Grp94-selective compounds inserted into site 2 when bound to Grp94 (Figure 1c).¹⁰ Selectivity for Grp94 over Hsp90 is achieved because the analogous site 2 is blocked in Hsp90. Not all ligands of this purine-scaffold class can access the site 2 pocket (Figure 2a–c). Those ligands that can access site 2 must be capable of adopting a “backward bent” conformation, whereas other ligands such as 5 adopt a “forward bent” conformation and bind to site 1 with no particular selectivity for the paralogs.¹⁰

■ LIGAND DESIGN, COMPUTATIONAL ANALYSES OF GRP94–LIGAND INTERACTION, AND BIOCHEMICAL TESTING

While our earlier work provided the rationale for the observed paralog selectivity, the detailed SAR of these purine-based inhibitors has not been described. Here, we discuss the design and synthesis of purine-based ligands that preferentially bind to site 2, which is unique to Grp94. Specifically, we report a tractable SAR of purine-based ligands that bind selectively and with varied degrees of affinity to the novel allosteric site 2 found only in Grp94. We focused our synthetic efforts on the exploration of various substituents on the C8-aryl ring (Figure 2d, substituents 2'–5'), the linker between the purine and the aryl moiety (Figure 2d, L), as well as at the N9/N3 position of the adenine core. We also explore the possibility of exchanging the N3 with a carbon atom, a modification claimed to improve

Scheme 1^a

^aReagents and conditions: (a) neocuproine, CuI, NaOt-Bu or Na₃PO₄ or K₂CO₃, DMF, 110 °C; (b) pent-4-yn-1-yl 4-methylbenzenesulfonate, Cs₂CO₃, DMF, 80 °C; (c) Cl(CH₂)_nCCH or Cl(CH₂)_nCN or Br(CH₂)_nCF₃ or Br(CH₂)_nC₆H₅, Cs₂CO₃, DMF, rt or 80 °C; (d) pent-4-yn-2-yl 4-methylbenzenesulfonate, Cs₂CO₃, DMF, 80 °C; (e) ROH, PPh₃, DBAD, CH₂Cl₂, toluene, rt.

Scheme 2^a

^aReagents and conditions: (a) *m*-CPBA, 30 min, rt; (b) P(OPh)₃, pyridine, microwave 220 °C, 30 min; (c) 5-chloropent-1-yne, Cs₂CO₃, DMF, 80 °C; (d) 2 equiv of Cs₂CO₃, DMF, 80 °C.

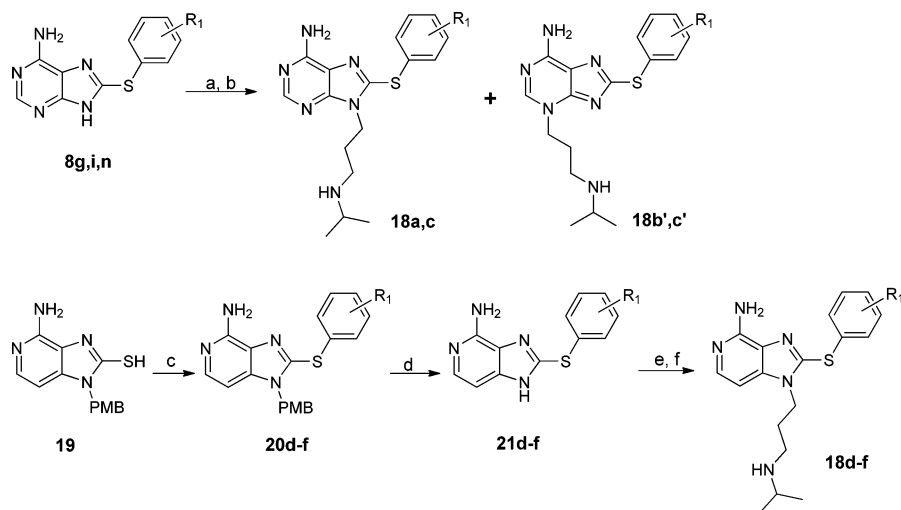
affinity for Hsp90 in the pan-Hsp90 inhibitor series.^{19,20} The design of these ligands is based on the resolved crystal structure of PU-H54 (4) with Grp94 (Figure 2b) and on the determined volume available for ligand binding inside site 2 (Figure 2c). The affinities of the synthesized compounds were determined using competitive binding assays to recombinant Grp94 protein.^{21,22} To determine the selectivity profile of our compounds, we also tested them for binding against purified Hsp90 α/β and Trap-1, using a published assay protocol.²² Further, to rationalize the affinity trends noted for these molecules and understand how the nature and size of substituents affect Grp94 binding, we used the reported X-ray crystal structures of PU-H54 (4) bound to the N-domain of Grp94 (PDB ID: 3O2F)¹⁰ to dock compounds into the allosteric binding site (site 2).

CHEMISTRY

8-Arylsulfanyl derivatives containing the N9-pent-4-yne chain were synthesized by utilizing a copper-catalyzed cross-coupling

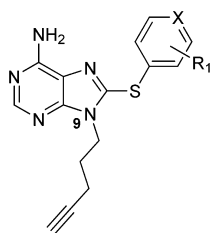
method previously described by us to generate key intermediates **8a–r,t–w** (Scheme 1).²³ Briefly, 8-mercaptoadenine (**6**) was reacted with various aryl iodides (**7**) using CuI/neocuproine as catalyst and NaOt-Bu (or Na₃PO₄ or K₂CO₃) as base in anhydrous DMF at 110 °C to generate 8-arylsulfanyl adenine intermediates (**8a–r,t–w**). Alkylation of **8a–r,t–w** with pent-4-yn-1-yl 4-methylbenzenesulfonate in the presence of Cs₂CO₃ yielded a mixture of N9-isomers (**9a–r,t–w**) and N3-isomers (**1** and **9a'–d',g',j'–n',q',v'–w'**)²⁴ in roughly 2:1 ratio, which were separated by preparative TLC. The synthesis of **9s** was carried out through a route that was previously described²⁵ from the reaction of 8-bromo-9-(pent-4-yn-1-yl)-9H-purin-6-amine²⁵ with 5-mercaptoisophthalonitrile²⁶ in the presence of *t*-BuOK in DMF at 130 °C.

The synthesis of compounds **13a–s** was carried out by alkylation of intermediate **8g** or **8n** with the appropriate alkyl alcohols under Mitsunobu conditions or alkyl halides or tosylates in the presence of Cs₂CO₃ to yield the desired N9-isomers after chromatographic separation (Scheme 1).

Scheme 3^a

^aReagents and conditions: (a) 3-(*tert*-butoxycarbonyl-isopropyl-amino)propyl tosylate, Cs₂CO₃, DMF, rt; (b) TFA, 0 °C; (c) ArI (7), neocuproine, CuI, NaO*t*-Bu or Na₃PO₄ or K₂CO₃, DMF, 110 °C; (d) TFA, 80 °C, 3 h; (e) 1,3-dibromopropane, Cs₂CO₃, DMF, 1.5–3h; (f) isopropylamine, DMF, rt.

Table 1



compd	R ₁	IC ₅₀ (μM)			
		Hsp90α	Hsp90β	Grp94	Trap-1
9a	2'-Cl	>100	>100	0.35 ± 0.05	ND
9b	2'-OCH ₃	>100	>100	6.2 ± 2.5	ND
9c	2'-CH ₂ OH	>100	>100	29.4 ± 9.1	ND
9d	2'-OCF ₃	>100	>100	1.4 ± 0.2	ND
9e	4'-OCH ₃	>100	>100	1.13 ± 0.2	ND
9f	4'-Cl	>100	ND	1.5 ± 0.2	ND
9g	2',4'-di-Cl	>300	>300	0.12 ± 0.04	145.4 ± 13.4
9h	2'-Cl,4'-Br	>50	ND	0.39	ND
9i	2',4'-di-CH ₃	>300	>300	1.63 ± 0.47	13.8 ± 1.8
9j	2',4'-di-OCH ₃	>50	>50	34.5 ± 3.5	ND
9k	2',5'-di-Cl	60.4 ± 1.6	>100	0.53 ± 0.10	5.1 ± 1.8
9l	2',5'-di-CH ₃	>300	>300	1.14 ± 0.14	203.7 ± 11.0
9m	2'-Cl,5'-CF ₃	>100	>100	0.5 ± 0.2	ND
9n	3',5'-di-Cl	>500	>500	0.26 ± 0.01	83.6 ± 11.8
9o	3'-Cl,5'-Br	>100	>100	0.24	ND
9p	3',5'-di-Br	>50	ND	0.29	ND
9q	3',5'-di-CH ₃	>300	>300	11.45 ± 0.92	157.9 ± 9.7
9r	2',6'-di-Cl-pyridine	8.3	ND	1.9	9.6
9s	3',5'-di-CN	>50	ND	7.73	ND
9t	3',4'-di-Cl	1.96	ND	0.695	ND
9u	2',3',4'-tri-Cl	15.97	39.47	0.430	3.60
9v	2',4',5'-tri-Cl	>200	>200	0.17 ± 0.11	78.4 ± 8.9
9w	2',4',6'-tri-CH ₃	>500	>500	2.1 ± 0.56	65.5 ± 1.3
5		0.043 ± 0.006	0.042 ± 0.003	0.026 ± 0.004	0.205 ± 0.006

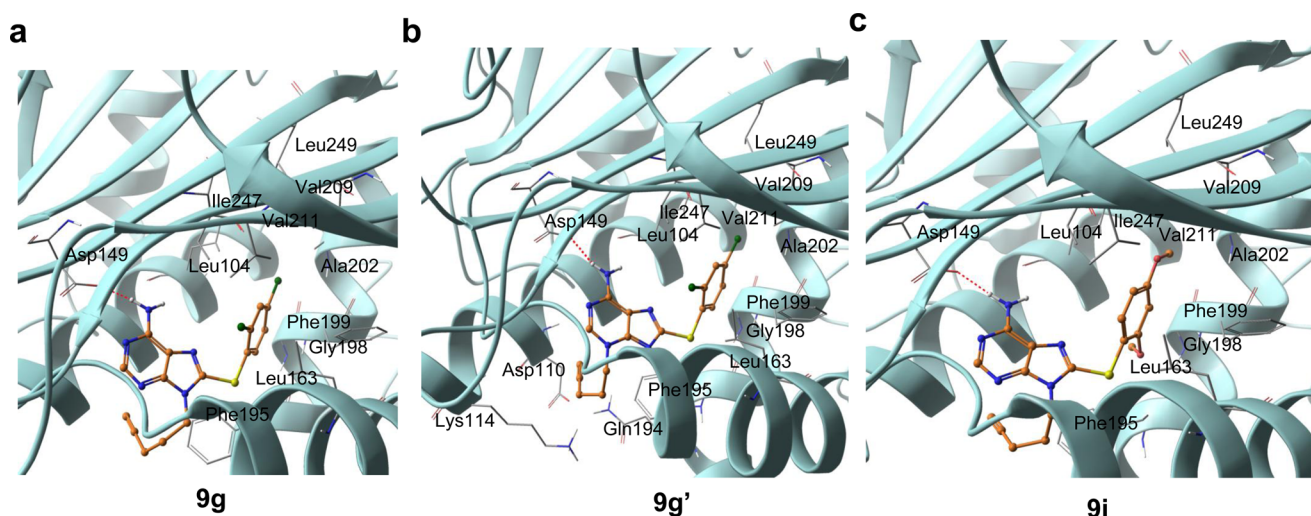


Figure 3. Predicted binding poses for **9g**, **9g'**, and **9i** when bound to the N-terminal domain of Grp94 (PDB ID: 3O2F).

The synthesis of analogs of **9g** with varying linker groups is shown in Scheme 2. Treatment of **9g** with 2 equiv of *m*-CPBA at rt yielded a mixture of sulfoxide **14a** and sulfone **14b**, in which each were readily isolated in 23% and 34% yield, respectively. The O-linked derivative **14c** was obtained from reaction of 8-bromo-9-(pent-4-yn-1-yl)-9H-purin-6-amine²⁵ with 2,4-dichlorophenol and KOt-Bu in 51% yield. Microwave-assisted cyclocondensation of 4,5,6-triaminopyrimidine (**15**) with 2,4-dichlorophenylacetic acid (**16**) yielded 8-benzyladenine **17** in 79% yield.²⁷ Heating a mixture of **17** with 1-chloropent-4-yne and 1.2 equiv of Cs₂CO₃ at 80 °C yielded **14d**, which could be converted to carbonyl derivative **14e** in 50% yield by heating at 80 °C with additional Cs₂CO₃.

Compounds having an ionizable 3-isopropylamino-propyl chain were synthesized by alkylation of 8-arylsulfanyl adenine intermediates **8g,i,n** with 3-(*tert*-butoxycarbonyl-isopropylamino)propyl tosylate in the presence of Cs₂CO₃, resulting in Boc-protected N9- and N3-regioisomers after separation.²⁸ Boc-deprotection of the N9- and N3-regioisomers in the presence of TFA yielded desired derivatives **18a,c** and **18b',c'** (Scheme 3), respectively. Related imidazopyridines **18d–f** (Scheme 3) were prepared using modifications to a synthetic route described earlier.²⁰ PMB-protected intermediates **20d–f** were obtained from CuI/neocuproine-catalyzed coupling of **19**²⁰ with various aryl iodides (**7**), which were then deprotected with TFA to yield **21d–f**. Alkylation of **21d–f** with 1,3-dibromopropane in the presence of Cs₂CO₃ followed by reaction with isopropylamine yielded imidazopyridines **18d–f**.

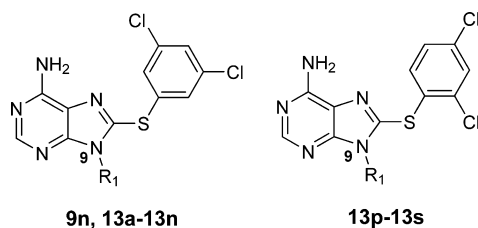
■ STRUCTURE–ACTIVITY RELATIONSHIP IN THE GRP94 INHIBITOR SERIES

Modifications on the 8-Aryl Ring. We began our SAR exploration by focusing first on substitutions on the 8-aryl ring (Figure 2d, substituents 2'–5') given that this region of the molecule can potentially occupy the hydrophobic site 2. Thus, with an interest in better understanding the polarity and volume of this pocket, a varied set of compounds was synthesized having substitutions on the 8-aryl ring focused primarily on the 2', 4', 2',4', 2',5', and 3',5'-positions, though other substitutions were also explored (Tables 1 and 4). A deleterious effect on activity was observed for more polar functionalities, as evidenced by compounds **9c** and **9r**, which further confirmed the hydrophobic profile of the pocket.

Interestingly, our SAR shows that the chlorine functionality is generally the preferred substituent in any combination as compared to other substituents explored, such as –OCH₃, –OCF₃, –CF₃, –CN, or –CH₃ (e.g., see **9a** vs **9b** and **9d**, or **9g** vs **9i**, or **9n** vs **9q** and **9s**), the only exception being bromine, which we find to be tolerable (see **9g** vs **9h**, or **9n** vs **9o** or **9p**). Although subtle electronic effects could play a role, we surmise that the size and lipophilicity of the chlorine atom are ideal to satisfy binding into the hydrophobic pocket site 2. In order to obtain a better understanding of this preference, as well as to provide further insight toward the design of more potent ligands, we next pursued docking studies.

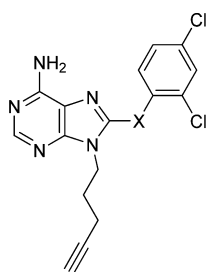
Indeed, in our docking analysis, chlorine at 2'-position is oriented nicely to form hydrophobic interactions with Leu163, Ile247, and Val211 (Figure 3a,b), which explains the higher binding affinity of **9a** for Grp94 over other substituents (i.e., **9b–d**). More polar substituents, as in **9b** (OCH₃), **9c** (CH₂OH), and **9d** (OCF₃), are less favorably oriented toward these hydrophobic residues and may account for the decrease in binding affinity. At the para-position, binding affinity appears to be less affected by substituent changes, as both –OCH₃ (**9e**) and –Cl (**9f**) at this position result in compounds with similar affinity (Table 1). Our findings suggest that while select purine analogs are indeed able to adopt the “backward bent” conformation and bind into site 2, the space available in the pocket is somewhat restricted at 2'-position, where smaller substituents are preferred, as evidenced by the drastic reduction in affinity observed for larger substituents. Our analysis of the effects of di- and trisubstitution on Grp94 affinity and selectivity further validated chlorine as the best substituent choice for the 8-aryl moiety. Briefly, dichloro substitutions at 2',4', 2',5', and 3',5'-positions on the 8-phenyl ring retained high affinity and selectivity but also indicated that 2',4'-substitution (i.e., **9g**) is preferred for higher affinity, followed by 3',5' (**9n**) and 2',5' (**9k**), as shown in Table 1. Concurrently, the same positions on the aryl ring substituted with methyl (**9i**, **9q**, and **9l**) reveal a significant loss of activity in the low micromolar range compared to the nanomolar affinity observed for the chlorine isomers. Additionally, the SAR also shows that 3',4'-disubstitution with chlorine (**9t**) is not as well-tolerated as 2',4' (**9g**), 3',5' (**9n**), and 2',5' (**9k**) given the observed loss in affinity and selectivity. Substitution of one of the chlorines with a bromine as in 2'-Cl,4'-Br (**9h**) and 3'-Cl,5'-Br (**9o**) as well as

Table 2



compd	R ₁	IC ₅₀ (μM)			
		Hsp90α	Hsp90β	Grp94	Trap-1
9n	-(CH ₂) ₃ CCH	>500	>500	0.26 ± 0.01	83.6 ± 11.8
13a	-(CH ₂) ₂ CCH	>50	>100	0.287	ND
13b	-(CH ₂) ₄ CCH	>50	>100	0.665	ND
13c	-CH ₂ CCCH ₃	>100	>100	5.1	ND
13d	-(CH ₂) ₂ CF ₃	>50	>100	0.56	ND
13e	-(CH ₂) ₃ CF ₃	>100	>100	0.502	ND
13f	-(CH ₂) ₄ CF ₃	>100	>100	2.74	ND
13g	-(CH ₂) ₅ CF ₃	>50	>100	1.648	ND
13h	-(CH ₂) ₃ CN	>50	>100	0.429	4.58
13i	-CH ₂ C ₆ H ₅	>50	>100	>5	ND
13j	-(CH ₂) ₂ C ₆ H ₅	>50	>100	>2.5	>100
13l	-CH(CH ₃)(CH ₂) ₂ CH ₃	>50	ND	14.3	ND
13m	-CH(CH ₃)CH ₂ CCH	>50	ND	5.8	ND
13n	-CH(C ₂ H ₅)CH ₂ CCH	>100	ND	>5	ND
13o	-(CH ₂) ₃ CH ₃	>50	ND	0.8	ND
13p	-CH(CH ₃)(CH ₂) ₂ CH ₃	>100	ND	2.48	>50
13q	-(CH ₂) ₂ CCH	>50	ND	0.39	7.23
13r	-CH(CH ₃)CH ₂ CCH	>50	ND	5.0	ND
13s	-CH(C ₂ H ₅)CH ₂ CCH	>50	ND	0.92	>50

Table 3



compd	X	IC ₅₀ (μM)			
		Hsp90α	Hsp90β	Grp94	Trap-1
9g	S	>300	>300	0.12 ± 0.04	145.4 ± 13.4
14a	S=O	24.9	ND	5.4	ND
14b	O=S=O	>25	ND	4.7	ND
14c	O	>100	ND	0.5	ND
14d	CH ₂	>100	ND	0.7	ND
14e	C=O	>100	ND	0.34	4.98

the dibrominated analog 3',5'-di-Br (**9p**) shows that bromine is well-tolerated at these positions. Combined, the available data proposed 3',5' and 2',4' as the optimal sites for substitution on the 8-aryl ring, yielding compounds with excellent selectivity and potency for Grp94.

In accordance with our previous findings, these compounds were each selective for Grp94. As mentioned above, the substitution pattern in these compounds was biased toward those that were known to favorably position the compound to

attain a backward bent conformation. This should not be taken to mean that these compounds cannot attain the forward bent conformation and potentially bind into site 1 present in Hsp90 (or Grp94 for that matter). These compounds are capable of attaining a forward bent conformation; however, the substituents chosen are known to not be ideal for binding into site 1 through previous SAR studies with Hsp90.²⁴ It can be envisioned that for any ligand there potentially exists an equilibrium whereby the 8-aryl group can adopt either a

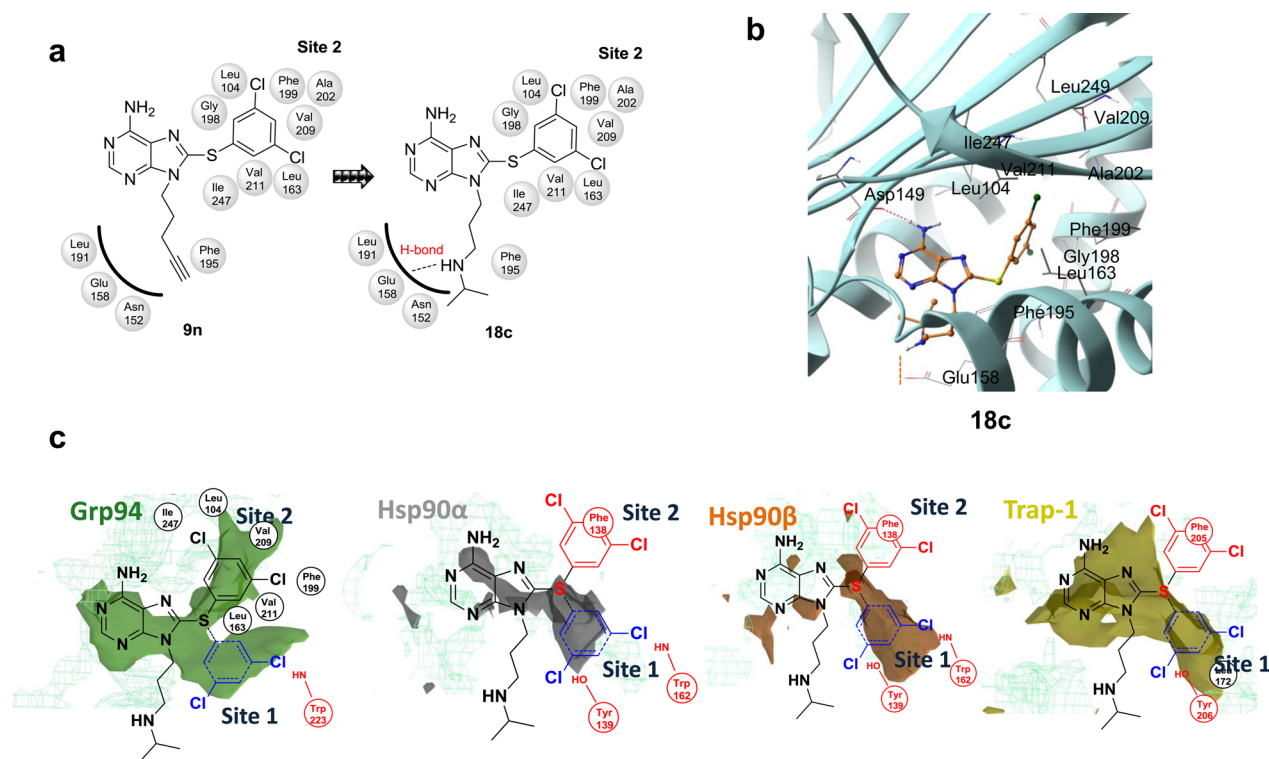


Figure 4. Design of 18c and its proposed interaction with the Hsp90 paralogs. (a) Interactions of 9n and 18c with the amino acids lining the Grp94 allosteric site 2. (b) Docking of compound 18c in the allosteric site 2 of Grp94. (c) Overlay of 18c on to sites 1 and 2 of the four Hsp90 paralogs. Residues that constrain either the availability of the site 2 pocket or the interaction of 18c with the protein are shown in red.

backward or forward bent conformation and thus occupy either site 2 or site 1, respectively. Energy minimization calculations show that certain ligands prefer a backward bent conformation and are thus favored entropically, but the difference in energy between these conformations is not enough to explain the observed selectivity. There is also an enthalpic component whereby stabilizing binding interactions that favor binding into one pocket over another are also necessary. The enhanced potency of ligands bearing more hydrophobic substituents is a direct consequence of the greater hydrophobic character of site 2 in Grp94. Combined, these two factors explain the high affinity and selectivity these ligands display for Grp94.

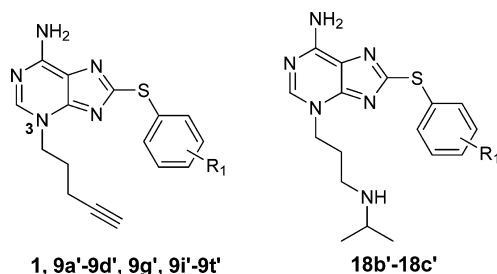
Modifications of the Linker between the Purine Core and the 8-Aryl Moiety. We next focused our efforts on examining the effect on potency and selectivity of the linker joining the purine core to the 8-aryl ring (Figure 2d). The adenine core binds in an essentially identical manner to each isoform, whereby a key interaction is formed between the exocyclic $-\text{NH}_2$ and N1 of the adenine with a conserved Asp149 of Grp94 (Asp93 of Hsp90 α/β , Asp158 of Trap1) and a network of water molecules at the bottom of the ATP-binding pocket.²² Since the adenine core is essentially static in binding to each of the isoforms, it is the linker atom that is a critical element to the ligand attaining the conformation necessary for selective Grp94 inhibition through binding into site 2. Naturally then, the linker group can be expected to have a significant impact on Grp94 binding/selectivity by impacting the dihedral angle, which is indeed the case (Figure S2, Supporting Information). Substitution of the S in 2',4'-di-Cl analog 9g with O (14c), CH_2 (14d), $\text{C}=\text{O}$ (14e), $\text{S}=\text{O}$ (14a), and $\text{O}=\text{S}=\text{O}$ (14b) was investigated by the synthesis of the corresponding analogs (Scheme 2). Substitution with O or CH_2 was tolerated, giving only a 4–6-fold decrease in activity;

however, this was not the case for the sulfoxide and sulfone derivatives, which showed a significant loss of activity (~ 40 -fold, Table 3). Overall, the sulfur linker was found to be the best choice, as it provided the most potent analog.

Modifications of the N3/N9-Substituents. We next examined the effect of different N9-substituents on Grp94 binding affinity and selectivity (Table 2). The appendage at the N9-position accommodated various chain lengths up to five carbons with a further increase resulting in a decrease in potency. Increasing the chain length from five to six carbons (9n vs 13b) at the N9-position resulted in approximately 3-fold decrease in potency for Grp94; however, a decrease in chain length to four carbons did not affect binding affinity (9n vs 13a). As seen in Figure 4a, the alkyne moiety of pent-4-ynyl (9n) and but-3-ynyl (13a) orients closer to Phe195 and makes critical π – π interactions, whereas hex-5-ynyl (13b) is unable to form such interactions because of its orientation away from this amino acid. As predicted by docking studies, moving the alkyne internally led to a decrease in Grp94 binding affinity (13a vs 13c, Table 2) which can be attributed to the inability of this compound to form π – π interactions with Phe195. Replacement of the alkyne with a trifluoromethyl group was also extensively investigated; however, this did not offer any improvement (see 13d–g, Table 2). Similarly, isosteric replacement of the alkyne with the more polar cyano group (13h, Table 2), while tolerated, does not offer any improvement over alkyne 9n. Introduction of bulkier substituents, such as benzyl (13i) and phenethyl (13j), result in a drastic decrease in affinity, caused most likely by steric clash with Phe195.

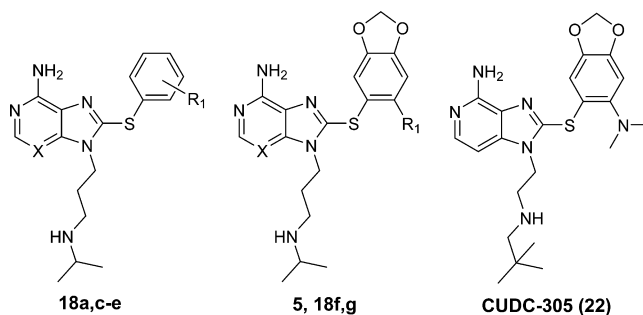
We had previously shown that C1'-substitution on the N9-substituent with a methyl group was a positive factor toward enhancing the selectivity of compounds for Grp94.¹⁰ In fact, this was one subtype of compound that was identified as

Table 4



compd	R ₁	IC ₅₀ (μM)				
		Hsp90α	Hsp90β	Grp94	Trap-1	Hsp90α/ Grp94
9a'	2'-Cl	>100	>100	100 ± 10	ND	—
9b'	2'-OCH ₃	>100	>100	>100	ND	—
9c'	2'-CH ₂ OH	>100	>100	>100	ND	—
9d'	2'-OCF ₃	>100	>100	>100	ND	—
9g'	2',4'-di-Cl	>500	>500	2.37 ± 0.79	9.6 ± 0.8	>210
4	2',4'-di-CH ₃	>250	>250	11.77 ± 3.24	54.1 ± 4.6	>21
9j'	2',4'-di-OCH ₃	>100	>100	>100	ND	—
9k'	2',5'-di-Cl	>100	>100	35.3 ± 5	ND	—
9l'	2',5'-di-CH ₃	>100	>100	>100	ND	—
9m'	2'-Cl,5'-CF ₃	>100	>100	>100	ND	—
9n'	3',5'-di-Cl	>100	>100	100 ± 8	ND	—
9q'	3',5'-di-CH ₃	>100	>100	>100	ND	—
9v'	2',4',5'-tri-Cl	>100	>100	2.08	19.5 ± 0.2	>48
9w'	2',4',6'-tri-CH ₃	>100	>100	20 ± 5	ND	>5
18b'	2',4'-di-CH ₃	>100	ND	>25	ND	4
18c'	3',5'-di-Cl	>100	>100	2.43	>100	>39
5		0.043 ± 0.006	0.042 ± 0.003	0.026 ± 0.004	0.205 ± 0.006	1

Table 5



compd	X	R ₁	IC ₅₀ (μM)			
			Hsp90α	Hsp90β	Grp94	Trap-1
18a	N	2',4'-di-Cl	20.3 ± 1.2	ND	0.41 ± 0.1	ND
18c	N	3',5'-di-Cl	27.3 ± 3.5	41.8 ± 1.3	0.22 ± 0.08	7.3 ± 0.5
18d	C	2',4'-di-Cl	>50	ND	3.44	14.1
18e	C	3',5'-di-Cl	>50	ND	1.08	7.2
18f	C	I	0.028	ND	0.101	ND
18g	N	N(CH ₃) ₂	0.100	ND	0.265	ND
5	N	I	0.043 ± 0.006	0.042 ± 0.003	0.026 ± 0.004	0.205 ± 0.006
22	—	—	33 ^a	38 ^a	190 ^a	1586 ^a

^aValues were obtained from ref 22.

Grp94-selective with greater than 10-fold selectivity over Hsp90α, Hsp90β and Trap1. Modeling indicated that the presence of a methyl group at this position favorably disposed the 8-aryl ring into the backward bent conformation. Because the substituents used to decorate the 8-aryl moiety were not particularly favorable for binding, these ligands were not potent

for Grp94. In contrast to Grp94 in this region, Hsp90 is characterized by a more limited volume, and indeed, previously reported SAR showed that C1'-substitution completely ablated Hsp90 binding.²⁹ Using this information, we had hoped to further enhance the selectivity for Grp94 through substitution at the C1'-position while at the same time incorporating the

favorable substituents that we show above to enhance potency (i.e., 2',4'-di-Cl and 3',5'-di-Cl). Unfortunately, it was not possible to ascertain the effects of such modification on selectivity, since at the highest concentration tested (maximal solubility) for these analogs (**13l–n,p,r,s**, Table 2) there was essentially no inhibition of Hsp90 α . However, the results do clearly show for both the butyl and butyne series that substitution with methyl (i.e., **13l,m,p,r**) or ethyl (i.e., **13n,s**) results in a decrease in potency for Grp94 relative to the unsubstituted analogs **13a,o,q**.

In addition to the N9-substituted compounds described above, we also examined the potency and selectivity of their N3-substituted analogs (Table 4), which were conveniently isolated as minor components in the syntheses of N9-compounds. We find that compared to the N9-series, N3-substituted compounds were considerably less potent (Table 4 vs Tables 1 and 5). In fact, because of solubility limitations an accurate IC₅₀ could not be determined for a number of the compounds. The compounds that we were able to evaluate, such as **9a'**, **9g'**, **4**, **9k'**, **9n'**, **9v'**, **9w'**, and **18c'** (Table 4), displayed a 10–400-fold decrease in affinity for Grp94. Importantly, the SAR of the N3-isomers correlated to that of the N9-alkylated series, since the 2',4'- and 2',5'-dichloro analogs were more potent than their dimethyl analogs (**9g'** vs **4** and **9k'** vs **9l'**, Table 4). Molecular docking studies suggested a distinct orientation and interaction of the N3- and N9-alkyl chain with Grp94. While the pent-4-ynyl moiety in the N9-position results in a bend that orients the chain closer to the surface of the protein to form hydrophobic interactions with Phe195 and Leu163 and π – π stacking with Phe195 (2.2 Å) of Grp94 (e.g., **9g**, Figure 3a), this is not the case for the N3-analogs, where the pent-4-ynyl moiety is positioned further away and orients instead to polar residues such as Lys114, Gln194, and Asp110, accounting for the decrease in binding affinity (**9g** vs **9g'**, Figure 3a,b).

As described above, our initial SAR focused on modification of the 8-phenyl ring and resulted in the identification of 2',4'- and 3',5'-dichloro-substituted analogs **9g** and **9n** (Table 1), respectively, as potent and selective Grp94 inhibitors. However, we found that these compounds had limited aqueous solubility and were less than optimal for use in cell-based studies and, moreover, difficult to formulate for in vivo studies. Therefore, in an attempt to improve aqueous solubility, we aimed to modify the N9-position based on our prior knowledge of the purine scaffold.²⁸ Additionally, the X-ray crystal structure of PU-H54 (**4**) with Grp94 reveals the presence of polar amino acids near the exit of the pocket that could potentially form H-bonds with a hydrophilic N9-substituent. On the basis of our earlier experience in the development of the pan-Hsp90 inhibitor PU-H71 (**5**), where the polar N9-amine projects out into the solvent, we decided to introduce the ionizable 3-isopropylamino-propyl group.²⁸ Gratifyingly for us, replacement of the pent-4-ynyl chain of **9g** and **9n** with the ionizable 3-isopropylamino-propyl chain provided derivatives **18a** and **18c**, which maintained the previously observed binding affinity for Grp94, though the 3,5-dichloro analog **18c** was slightly better than the 2,4- compound **18a**. As such, **18c** shows good potency for Grp94 (IC₅₀ = 0.22 μ M) and selectivity over other paralogues (>100- and 33-fold for Hsp90 α/β and Trap-1, respectively, Table 5). Additionally, **18c** can be formulated as either a mesylate or hydrochloride salt, which increases its water solubility (i.e., >10 mg/mL).

To rationalize the binding affinity, we docked compound **18c** into the binding site of Grp94 (Figure 4b, PDB ID: 3O2F). Unlike the hydrophobic chain of **9n**, the polar chain at N9 orients away from Phe195 (Figure 4a,b) and is predicted to form hydrogen bonds with surface amino acids such as Glu158 in Grp94, which seems to compensate for the loss of hydrophobic and π – π interactions with Phe195, resulting in a similar inhibition profile (**18c** vs **9n**, Tables 5 and 1). To determine the reason for ligand selectivity, sites were generated by SiteMap using a previously described procedure¹⁰ on each protein, and the sites were overlaid onto the structure of **18c** (Figure 4c). In Grp94, there are two sites available for the right side phenyl ring to orient into (sites 1 and 2). The phenyl ring of **18c** orients into energetically favorable site 2 (backward bent) and is stabilized by hydrophobic interactions with Leu104, Leu163, Phe199, Ala202, Phe203, Val211, Ile247, and Leu249. Orientation of **18c** into site 1 of Grp94 was less preferred due to energy constraints and unfavorable interactions with Trp223 (NH). The ability of compound **18c** to access site 2 and favorably bind in this pocket results in the observed high affinity of this ligand for Grp94. Only site 1 is available for the phenyl ring to orient into in Hsp90 α , Hsp90 β , and Trap-1 (Figure 4c) since a steric clash of the phenyl ring with Phe138 (Hsp90 α/β) or Phe205 (Trap-1) would preclude binding into site 2. This restriction as well as unfavorable interactions of the hydrophobic substituents of **18c** (3,5-di-Cl) with polar amino acids of site 1 [i.e., Trp162 (NH) and Tyr139 (OH) in Hsp90 α/β and Tyr206 (OH) in Trap-1] results in low-affinity binding to Hsp90 α/β and Trap-1 and the resulting selectivity for Grp94.

Modification of the Purine Core—Substitution of N3 with C. In an attempt to explore further structural modifications that might improve pharmacological properties, we sought to modify the 3-position nitrogen of the purine to a carbon, as shown in Scheme 3. Previously, such a modification was utilized by researchers at Curis in the development of Hsp90 inhibitors, since they had rationalized that the N3 nitrogen lacks direct contact with Hsp90, although it does make water-mediated hydrogen bonds with Gly97 and Asp102.³⁰ The resulting imidazopyridines are reported to bind to Hsp90 with high affinity,^{19,20} and one of these analogs, CUDC-305 (**22**; Table 5), is in clinical trials for cancer. Since such a change would be expected to alter the physicochemical properties, we sought to make a similar modification to **18a** and **18c**. Somewhat surprisingly, we found that such a change substantially diminished potency (5–8-fold for **18d** and **18e**) for Grp94, indicating that the N3 is significant for binding of **18a** and **18c** to Grp94. Examination of the crystal structure for PU-H54 (**4**) bound to Grp94 was not much help for us in understanding the role of N3, since this analog is N3-substituted and would alter the H-bond capabilities of the nitrogen by diminishing electron density as well as sterically affecting it. Therefore, we relied upon the crystal structure of NECA (**1**) bound to Grp94, which shows that N3 forms water-mediated H-bonds with Asn162 and Lys114 (Figure S3, Supporting Information) in a manner highly similar to that observed for PU-H71 (**5**) bound to Hsp90.³⁰ Therefore, on the basis of this as well as our binding results between the two series (i.e., **18a** vs **18d**, and **18c** vs **18e**, Table 5), water-mediated hydrogen bonds made with the ligand through N3 are significant for affinity (Figure S3, Supporting Information).

Previously, when we had compared the binding mode of some pan-inhibitors to the various isoforms of Hsp90, we found

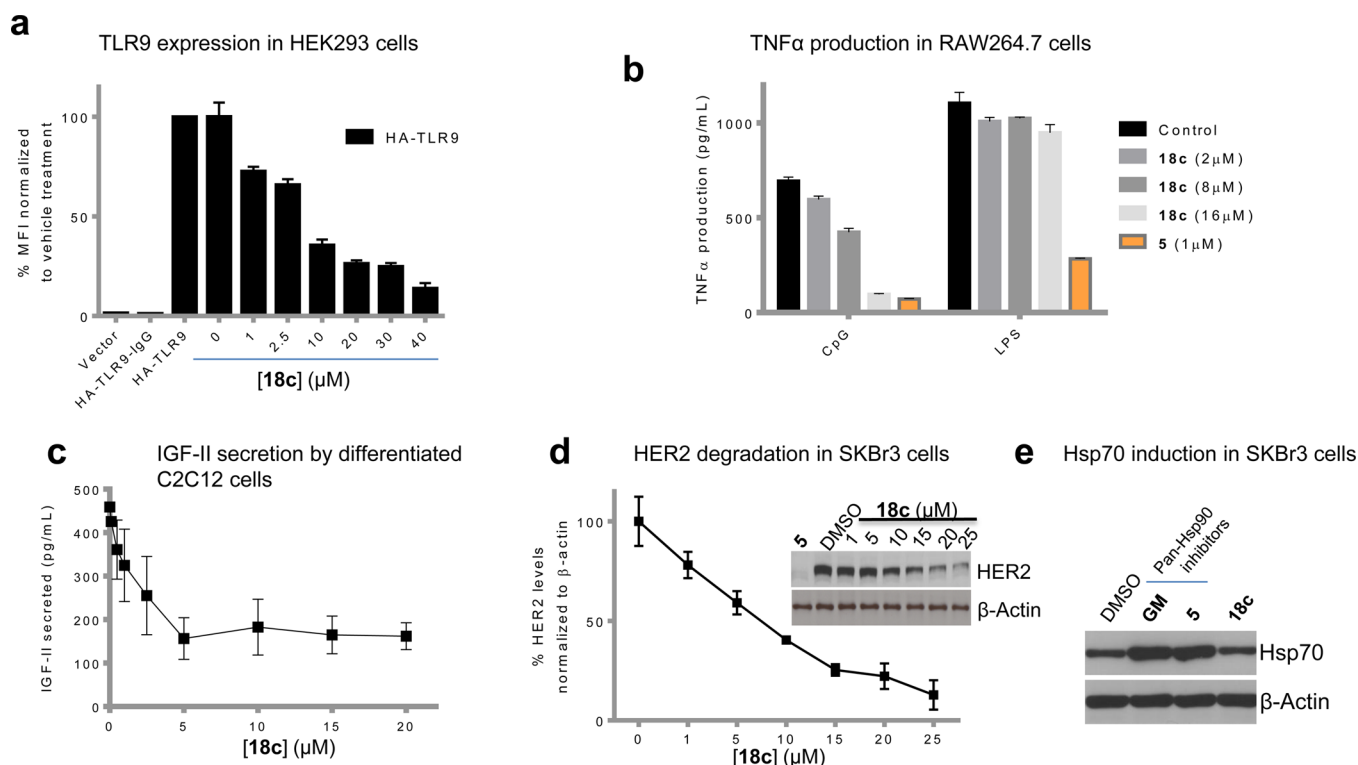


Figure 5. Grp94-specific inhibitor **18c** dose-dependently inhibits several Grp94-mediated cellular effects, such as (a) TLR9 expression, (b) TNF α production in cells stimulated with CpG, (c) IGF-II production by differentiated myoblasts, and (d) HER2 degradation in HER2-overexpressing breast cancer cells. Selectivity of **18c** for Grp94 over the cytosolic Hsp90 is demonstrated by the lack of activity in cells stimulated by LPS (b) and no Hsp70 induction in SKBr3 cells (e), both effects mediated by Hsp90. PU-H71 (**5**) and GM are pan-Hsp90 inhibitors (i.e., bind equally well to both Grp94 and the cytosolic Hsp90s). Data points are mean \pm error, $n = 4$.

that the affinity of CUDC-305 (**22**) for Grp94 ($IC_{50} = 190$ nM) was ~ 6 -fold lower than for Hsp90 α ($IC_{50} = 33$ nM) or Hsp90 β ($IC_{50} = 38$ nM).²² This was attributed by modeling to be due to steric clashes that occur between the dimethylamine group with Phe195 and Leu163 in the Grp94 binding pocket.²² The significance of a nitrogen or carbon at the 3-position of the adenine ring was not considered at the time. In order to further elucidate the effects of such substitution we prepared both the dimethylamine analog (**18g**) and the C3 analog (**18f**) of the pan-inhibitor PU-H71 (**5**). We chose to make analogs of PU-H71 (**5**) because of the similar affinity this compound displays for Grp94 and Hsp90 α/β , which would allow us to more carefully gauge such effects. Substitution of the iodine with dimethylamine (**18g**) resulted in a similar decrease (~ 3 -fold) in relative affinity for Grp94 that is observed with CUDC-305 (**22**), and when compared to PU-H71 (**5**), substitution results in a 10-fold loss of affinity for Grp94, supporting the notion of a steric clash that was earlier suggested by modeling. Similarly, the C3 analog of **5**, **18f**, displayed ~ 4 -fold lower affinity for Grp94 compared to Hsp90 α and when compared to PU-H71 (**5**), further supporting the importance of N3 for binding to Grp94.

BIOCHEMICAL AND BIOLOGICAL EVALUATION OF THE GRP94 LIGANDS

Off-Target Selectivity Testing. Because these ligands are based on a purine scaffold, there is the misconception that they tend to nonspecifically interact with ATP-binding pockets, such as those of kinases. Both derivative **18c** and **9g** were tested at 10 μ M against the scanEDGE 97 kinase panel (Figure S4,

Supporting Information). This panel contains a set of kinases covering AGC, CAMK, CMGC, CK1, STE, TK, TKL, lipid, and atypical kinase families, plus important mutant forms. Developed by Ambit Biosciences, it employs proprietary active-site-dependent competition binding assays to determine how compounds bind to kinases.³¹ It is based on a competition binding assay that quantitatively measures the ability of a compound to compete with an immobilized, active-site-directed ligand and can be used in detection of multiple inhibitor types (e.g., type I, type II, and non-ATP competitive). Compound **18c** was inert against the kinase panel, while only two minor interactions were identified for compound **9g** (MKNK2 and ROCK2, 34% and 32% inhibition, respectively) (Figure S4, Supporting Information).

Biological Evaluation of Grp94 Selectivity in Cells. We next addressed the paralog specificity of these compounds in a cellular system because the biochemical affinity and selectivity of these compounds measured *in vitro* with recombinant protein may differ from their effects on Hsp90 paralogs within cells. There are multiple factors that could contribute to such a profile, including differences in the cellular abundance and distribution of the Hsp90 paralogs. Additionally, post-translational modifications (PTMs) and complex formation of intracellular Grp94 could potentially render a distinct inhibition profile to that observed compared to recombinant protein.³² Thus, to confirm that these compounds act in cells through paralog-specific inhibition, we tested the selective target modulation of compound **18c** by several functional readouts.

TLRs are a family of pattern recognition receptors for pathogens that have critical roles in innate immunity against infection.³³ Thirteen TLRs exist in mammals and they localize

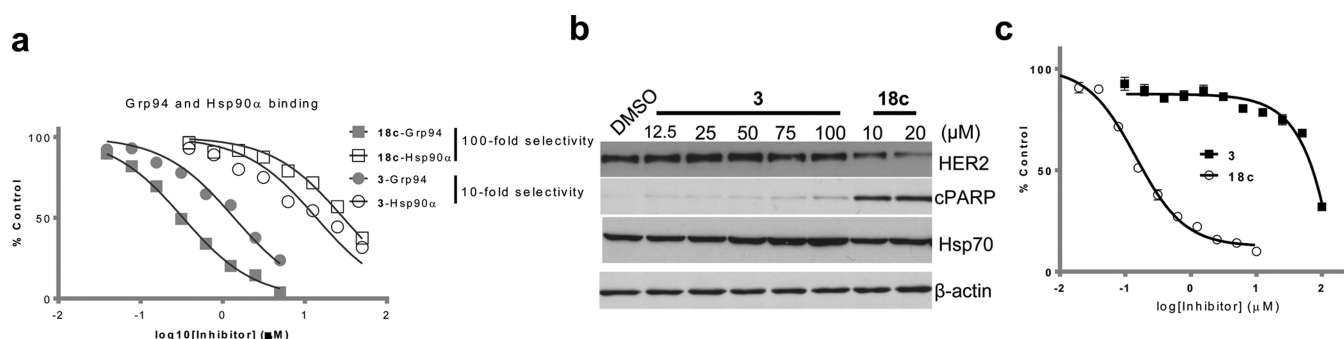


Figure 6. (a) Relative binding affinity of Grp94 inhibitors for Hsp90 α and Grp94 was measured using a fluorescence polarization assay as previously reported.²² (b) The HER2-overexpressing breast cancer cells SKBr3 were treated for 24 h with the indicated concentrations of Grp94 inhibitors, and proteins were analyzed by Western blot. Representative blots of triplicate experiments are shown. (c) Viability of cancer cells treated for 72 h with the indicated Grp94 inhibitor concentrations was measured using the CellTiter-Glo cell viability assay. Data points are mean \pm error, $n = 4$.

either on the cell surface or in the endolysosome compartment. Grp94 is one of several accessory proteins that regulate intracellular trafficking of TLR9. In the absence of Grp94 or when Grp94 chaperoning function is inhibited pharmacologically, TLR9 fails to exit the endoplasmic reticulum, and therefore, Grp94-deficient macrophages fail to recognize unmethylated CpG DNA and induce TNF- α production.³⁴ Impairment of Grp94 function increases the proteolytic sensitivity of TLR9, possibly because, in the absence of Grp94, TLR9 is not folded properly and is turned over in the ER or secretory pathways. Indeed, **18c** dose-dependently inhibited the expression of TLR9 in the post-ER compartment (Figure 5a) and the CpG induced TNF- α production (Figure 5b). **18c** also dose-dependently inhibited IGF-II secretion by differentiated myoblasts (Figure 5c) and reduced the steady-state levels of HER2 kinase in HER2 overexpressing breast cancer cells (Figure 5d), both Grp94-mediated cellular processes.^{10,35}

While these functional readouts confirm Grp94 inhibition in cells by **18c**, they do not exclude potential interference with Hsp90, the cytosolic paralog. Therefore, we also investigated the ability of **18c** to modulate Hsp90-specific functions (Figure 5e). One such function is related to Hsp90's ability to maintain the transcription factor HSF-1 sequestered to the cytosol, where it directly binds to it and prevents its activation.³⁶ When Hsp90 is inhibited, HSF-1 is released from Hsp90, trimerizes to an active transcription factor, and translocates to the nucleus to bind to several promoters of heat-shock proteins, resulting in increased transcription and synthesis of these proteins, such as Hsp70. Indeed, inhibition of Hsp90, by either the Hsp90-selective inhibitor PU29F¹⁰ or by the pan-Hsp90 inhibitors GM^{37,38} or PU-H71,^{28,39} led to upregulated levels of Hsp70. As a confirmation of its retained paralog specificity in cells, **18c** did not modulate this Hsp90-related event at concentrations that resulted in Grp94 inhibition in cells.

Distinct Grp94 Inhibitors May Result in Nonoverlapping Phenotypes. Molecular chaperones are atypical drug targets because they can exist as fluid complexes. They can exist in cells as components of complexes bound to nucleotide, cochaperone, or client proteins and are subject to PTMs.³² Combined these two factors help to regulate chaperone function and enable the cell to mount a stress response as is needed under diverse cellular conditions. These can also serve to explain the differences observed with different inhibitors. For instance, there is a significant difference observed both at the biochemical and at the cellular level for Hsp90 inhibitors that

target the N-terminal domain from those that target the C-terminus of Hsp90.^{40,41} There is even considerable difference observed in vitro and in vivo between those inhibitors that target the N-terminal nucleotide binding pocket.^{42–44} Despite sharing a similar binding site, these inhibitors can display significantly different properties, and it seems that no two inhibitors are the same as a result of their ability to sample different conformations and chaperone complexes.³²

In this context, we were intrigued by the previous observation that BnIm (**3**) lacked antiproliferative effects against HER2-overexpressing SKBr3 cells.¹⁷ This contrasted with our findings that inhibition of Grp94 by **18c** or knock-down of Grp94 by siRNA led to growth impairment in these cells.¹⁰ In order to directly compare the effects of these two classes of compounds, we synthesized **3** according to published procedures.^{16,17} As noted above, **3** binds into site 3 (Figure 1b), in contrast to **18c**, which binds into site 2. While the IC₅₀ of **3** for Grp94 is reported,¹⁸ its specificity for the other Hsp90s was not specified, so the potency and selectivity against recombinant protein could not be clearly assessed. Although in silico docking predicted for **3** a binding mode that oriented the benzyl ring into the pocket of Grp94, no crystal structure was provided to confirm this hypothesis. The selectivity of **3** for Grp94 was hypothesized on the basis of cell-based functional assays that were interpreted to be readouts of specific Grp94 or Hsp90 α/β function, and the precise paralog selectivity/potency profile of **3** remains unclear.

Thus, we first chose to determine both the potency and selectivity of **3** against Grp94 and Hsp90 α . We obtained an IC₅₀ of 1.2 and 14 μ M for Grp94 and Hsp90 α , respectively (\sim 12-fold selective) (Figure 6a). The binding affinity of **3** for Grp94 is similar to that recorded for this compound (IC₅₀ = 1.5 μ M).¹⁸ Next, we tested the effect of BnIm on HER2, a protein that we have recently shown to be dependent on Grp94 in SKBr3 cells.¹⁰ Specifically, we demonstrated that the stability and function of HER2 at the plasma membrane of tumor cells characterized by high HER2 expression are critically regulated by Grp94.¹⁰ Consistent with previous results,¹⁷ we observed no effect of **3** in SKBr3 cells up to 10 μ M, a concentration previously reported to inhibit both TLR9 trafficking and IGF-II secretion.¹⁷ We increased the concentration of BnIm to 100 μ M, a concentration recently shown to inhibit the chaperoning of myocilin by Grp94.¹⁸ At 100 μ M, a slight effect could be seen for **3** on SKBr3 cells, as noted by minor PARP cleavage and possibly a slight reduction in HER2 (Figure 6b) and by cellular toxicity (Figure 6c); this, however, we could not

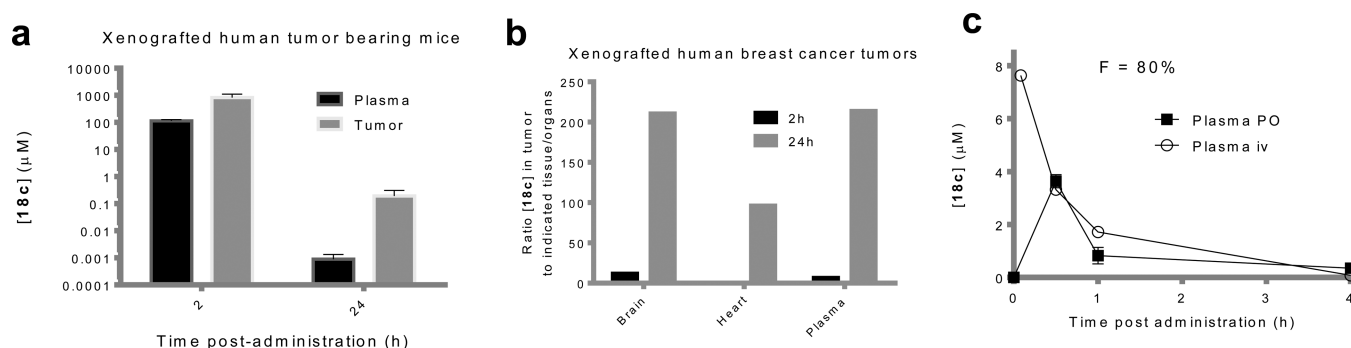


Figure 7. In vivo profile of **18c**. (a) **18c** (75 mg/kg, ip) was administered to mice ($n = 4$ per experimental point) bearing breast tumors, and mice were sacrificed at 2 and 24 h postadministration. Inhibitor levels in the indicated tissues and plasma were determined by LC–MS/MS following administration of **18c**. Each data point represents the mean \pm error. (b) The concentrations of **18c** in tumor to brain, heart, and plasma of mice as in panel a were determined by LC–MS/MS and the ratios plotted. (c) **18c** was injected as a single dose iv or oral at 10 mg/kg to B6D2F1 mice ($n = 2$ male mice per experimental point, 20 mice total). The agent was formulated in 30% captisol, 5 mM citrate buffer at pH 4.2. Agent levels ($\mu\text{g/g}$ or $\mu\text{g/mL}$) were determined by LC–MS/MS and converted to molar concentrations with the approximation that $1\text{g} = 1\text{mL}$. Concentrations were graphed against the time of sacrifice, which represents the time after agent administration. Each point represents mean \pm error.

specifically attribute to Grp94 inhibition, because at this concentration Hsp70 induction (indicating cytosolic Hsp90 inhibition) was also noted (Figure 6b).

Through these data we cannot conclusively attribute the lack of effect for **3** in SKBr3 cancer cells on its distinct binding interaction with Grp94; while we favor an explanation that diverse binding modes may enable each compound to sample a diverse range of conformations, resulting in different phenotypes, other mechanisms such as an inability of **3** to access Grp94 at the plasma membrane (such as Grp94 being translocated in SKBr3 to chaperone HER2¹⁰) might also account for the phenotypic differences. Nonetheless, these results demonstrate that the effect of small-molecule inhibition of Grp94 is context-dependent and suggests that future efforts in the development of Grp94 inhibitors should implement, in addition to biochemical tests, relevant phenotypic and cell-specific target modulation assays.

In Vivo Pharmacokinetics. So far there is no report on the in vivo profile of a Grp94 inhibitor. Studies conducted with pan-Hsp90 inhibitors indicate a tumor-targeting and retention profile for such compounds.^{32,39} This was rationalized by the existence of Hsp90 species in tumors distinct from those expressed in normal cells.^{32,42,45} Specifically, the presence of aberrant proteins, such as those present in cancer cells, may shunt Hsp90 to a highly cochaperone bound and dependent complex that exhibits high affinity not only for its endogenous ligand, ATP, but also for ligands that occupy the ATP pocket. This stress-specific Hsp90 complex we termed the oncogenic Hsp90 species.⁴² In contrast, in normal cells, Hsp90 exists in complexes of dynamic nature that regulate normal cell physiology, also termed housekeeping Hsp90 species.

To address the question whether a tumor-specific retention profile may also extend to the allosteric Grp94 inhibitors described here, we performed a pilot PK study for **18c** (Figure 7). No acute toxicity was observed upon intraperitoneal administration of the agent to mice at doses as high as 150 mg/kg (higher was not tested due to solubility limitations). In this PK study we incorporated two time points, a 2 and 24 h time of sacrifice postadministration (Figure 7a). The early time point is incorporated to test the biodistribution of the agent to the site of its action, the tumor; **18c** was readily distributed to tumor mass with $\sim 850\ \mu\text{M}$ noted in tumor at 2 h vs $100\ \mu\text{M}$ in the plasma. At 24 h, the ratio of agent in tumor vs plasma

increased to 200:1 and the tumor vs heart to 100:1, indicating specific retention of **18c** in the tumor mass (Figure 7b). We further validated our findings in B6D2F1 mice, in which we conducted a “classical” pilot PK study (Figure 7c). The fraction of agent that reached systemic circulation (F) after oral administration was 80%, which is suggestive of good absorption and limited first-pass metabolism (Figure 7c). This study reinforces our findings in the tumor-bearing mice; specifically, we see a high C_{max} , AUC, and % F (po) in the plasma in the time interval of 0–4 h, which is in accord with the rapid and good biodistribution we determined above (Figure 7a). These studies are encouraging, as they indicate that we have a very good pharmacophore and lead compound in **18c**. They also suggest that specific tumor targeting with rapid clearance from normal tissue is also possible in the Grp94 purine-scaffold series, similarly to that observed for the purine-scaffold pan-Hsp90 inhibitors.^{46–49}

CONCLUSIONS

This report is the first to describe a comprehensive SAR of Grp94 inhibitors that interact with the allosteric site 2 and to offer valuable insight into ways to overcome the high structural similarity among Hsp90s in the ligand-binding pocket. Whereas previous efforts in the field provided useful information on the feasibility of achieving selectivity for this Hsp90 isoform, the current work provides detailed knowledge on the ligand characteristics required for selective Grp94 inhibition both in vitro and in cells. It also presents several context-dependent biological assays that probe binding to Grp94 in cellular models of disease and thus provides a blueprint for future medicinal chemistry efforts. Not last, it provides preliminary in vivo testing of a Grp94 inhibitor to suggest specific and effective targeting of tumors by a Grp94 ligand.

In this paper we describe the design and synthesis of purine-based ligands that preferentially bind to site 2, which is unique to Grp94, and confers selectivity over other paralogs. Specifically, this work resulted in compounds such as **18c**, which shows good binding affinity for Grp94 and selectivity over the other Hsp90 paralogs. To come to this conclusion, we synthesized, characterized, and tested approximately 70 ligands that together encompass nine points of variation on the pharmacophore. As such, we extensively probed substitutions on the 8-aryl, the nature of the linker between the purine ring

and the 8-aryl, and the nature and length of linkers attached at either N3 or N9 of the purine, and last, we modified the purine core itself by replacing N3 with a carbon.

We also provide here a rationale for the preferred chemical spaces that elicit a “backward bent” that is directed toward the unique binding site of Grp94 and optimally complements volume and polarity characteristics of the site 2 binding pocket to result in high affinity binding. The conformation observed for the binding of these ligands to Grp94 is distinct from all previous structures (apo and ligand bound) reported for Grp94 and it is important to note that this novel pocket (site 2) becomes exposed and subsequently available for binding only after ligand-induced conformational changes to Grp94. Upon interaction, compounds such as those described here are capable of inducing a conformational change in Grp94 that results in the exposure of a unique binding pocket that can then be filled by the ligand.

We further validated that **18c** acts in cells through Grp94-specific inhibition using a number of functional readouts. Specifically, we show that **18c** inhibits both the post-ER expression of TLR9 as well as CpG-induced/TLR9-mediated TNF- α production. **18c** also inhibits IGF-II secretion by differentiated myoblasts and reduces the steady-state levels of HER2 kinase in HER2-overexpressing breast cancer cells. At these Grp94-modulatory concentrations, we show that **18c** has no effects on Hsp90-mediated functions in cells, providing proof for its in cell selectivity.

We also present data comparing the activity of two Grp94 classes and show that the phenotypes of the two compounds do not necessarily overlap. As the field is coming to appreciate, chaperones regulate proteins by co-opting activating cochaperones and adapter proteins. In disease, these complexes are context-dependent, in that they form to buffer the specific alterations in the proteome. The efficacy of an agent targeting a chaperone in these cells is therefore determined by its ability to sample and engage such complexes, stressing the need to test chaperone inhibitors in the disease context they are therapeutically developed for.

We also provide for the first time information regarding the in vivo profile of a selective Grp94 inhibitor. When administered to tumor-bearing mice, **18c** was cleared relatively rapidly from normal tissue while being selectively retained in tumor; this is remarkable considering that Grp94 is similarly expressed in most tissues and organs. Such phenomenon was previously observed with pan-Hsp90 inhibitors.^{32,39,40} It is believed that the tumor-specific effects of HSP inhibitors are due to an activation of the chaperones in tumors by factors such as proteotoxic stress. Because of these features, and like the Hsp90 inhibitors, it is not envisioned that Grp94 inhibitors will be targeted systemically but, rather, will show preferential localization in tumors. We have confirmed these concepts with our pharmacokinetic data.

It is yet unclear whether such a tumor-retention feature extends to all Grp94 pharmacophores. For Hsp90 inhibitors it was determined that not all inhibitors exhibit such preference for tumor species, possibly because not all inhibitors interact with the protein in an identical fashion.⁴² Each inhibitor may preferentially sample specific conformations and complexes of the HSP, and it is expected that those that sample preferentially the tumor, active complexes would be those with higher therapeutic index.³² This remains to be seen as more Grp94 inhibitor classes move to in vivo studies.

In summary, our findings suggest Grp94 as a valid target for therapeutic intervention and position the Grp94 inhibitors such as **18c** as therapeutic leads in the development of drugs for the treatment of immune-related disorders and certain cancers.

EXPERIMENTAL SECTION

Chemistry. ¹H and ¹³C NMR spectra were recorded on a Bruker AV-III 400, 500, or 600 MHz NMR spectrometer. Chemical shifts are reported in δ values in ppm downfield from TMS as the internal standard. ¹H data are reported as follows: chemical shift, multiplicity (s = singlet, d = doublet, t = triplet, q = quartet, br = broad, m = multiplet), coupling constant (Hz), integration. ¹³C chemical shifts are reported in δ values in ppm downfield from TMS as the internal standard. High-resolution mass spectra were recorded on a Waters LCT Premier system. Low-resolution mass spectra were obtained on Waters Acquity Ultra Performance LC with electrospray ionization and SQ detector. The purities of title compounds were determined by analytical HPLC, performed on a Waters Autopurification system with PDA, MicroMass ZQ and ELSD detector, and a reverse-phase column (Waters X-Bridge C18, 4.6 \times 150 mm, 5 μ M) using method A [(a) H₂O + 0.1% TFA and (b) CH₃CN + 0.1% TFA, 5 to 95% b over 10 min at 1.2 mL/min] or method B [(a) H₂O + 0.1% TFA and (b) CH₃CN + 0.1% TFA, 20 to 90% b over 16 min at 1.0 mL/min]. Title compounds used were >95% pure. Analytical thin-layer chromatography was performed on 250 μ M silica gel F₂₅₄ plates. Preparative thin layer chromatography was performed on 1000 μ M silica gel F₂₅₄ plates. Flash column chromatography was performed by employing 230–400 mesh silica gel. Solvents were HPLC grade. PU-H71 (**5**) was synthesized as previously reported.²⁸ The synthesis of **18g** is described in the Supporting Information. CUDC-305 (**22**) was purchased from ChemieTek.

General Procedure for Synthesis of 8-Arylsulfanylpurines (8). 8-Mercaptoadenine (**6**); corresponding aryl iodide **7** (300 mol %); neocuproine hydrate (10 mol %); CuI (10 mol %); NaOt-Bu, K₂CO₃, or Na₃PO₄ (200 mol %); and DMF (2 mL) were charged in a dry vessel under nitrogen atmosphere. The reaction vessel was sealed and placed in an oil bath (110 °C) and stirred for 24 h. The reaction mixture was then cooled to room temperature and DMF was removed in vacuo. The crude material was purified by silica gel flash chromatography eluting with a gradient of CH₂Cl₂:CH₃OH:CH₃COOH at 60:1:0.5 to 20:1:0.5 to afford the desired products.

8-((3-Bromo-5-chlorophenyl)thio)-9H-purin-6-amine (8o). Yield: 42%. MS (ESI): m/z 356.1/358.1 [M + H]⁺.

8-((3,5-Dibromophenyl)thio)-9H-purin-6-amine (8p). Yield: 40%. MS (ESI): m/z 401.9 [M + H]⁺.

8-((2,6-Dichloropyridin-4-yl)thio)-9H-purin-6-amine (8r). Yield: 50%. MS (ESI): m/z 312.8 [M + H]⁺.

8-((3,4-Dichlorophenyl)thio)-9H-purin-6-amine (8t). Yield: 69%. MS (ESI): m/z 312.0 [M + H]⁺.

8-((2,3,4-Trichlorophenyl)thio)-9H-purin-6-amine (8u). Yield: 43%. MS (ESI): m/z 347.7 [M + H]⁺.

8-(Mesitylthio)-9H-purin-6-amine (8w). Yield: 53%. ¹H NMR (400 MHz, DMSO): δ 13.1 (br s, 1H), 8.02 (s, 1H), 6.93–7.04 (m, 5H), 2.33 (s, 6H), 2.25 (s, 3H). MS (ESI): m/z 286.1 [M + H]⁺.

Synthesis of **8a–n**, **8q**, and **8v** followed a similar protocol. The synthesis and characterization of these coupling products have been described elsewhere.²⁴

General Procedure for the Synthesis of 9 and 9'. A mixture of 8-arylsulfanyladenine **8** (100 mmol), Cs₂CO₃ (100 mmol), and pent-4-ynyl 4-methylbenzenesulfonate (120 mmol) in DMF (1.3 mL) under nitrogen atmosphere was heated at 80 °C for 30 min. Following solvent removal, the crude material was purified by preparatory TLC with CHCl₃:MeOH:NH₄OH at 10:1:0.5 or CHCl₃:MeOH:AcOH at 10:1:0.5 to provide the corresponding 9-alkyl-8-arylsulfanyladenine derivatives **9** and 3-alkyl-8-arylsulfanyladenine derivatives **9'**.

8-(2-Chlorophenylthio)-3-(pent-4-ynyl)-3H-purin-6-amine (9a'). Yield: 10%. ¹H NMR (400 MHz, CDCl₃/MeOH-*d*₄): δ 8.02 (s, 1H), 7.48–7.51 (m, 1H), 7.40–7.42 (m, 1H), 7.14–7.17 (m, 2H),

4.49–4.51 (m, 2H), 2.17–2.22 (m, 4H), 2.05–2.06 (m, 1H). MS (ESI): m/z 344.0 [M + H]⁺. HRMS (ESI): m/z [M + H]⁺ calcd for C₁₆H₁₅N₅ClS 344.0737, found 344.0720. HPLC: (b) t_R = 7.84 min, 99.6%.

8-(2-Methoxyphenylthio)-3-(pent-4-ynyl)-3H-purin-6-amine (9b'). Yield: 25%. ¹H NMR (400 MHz, CDCl₃/MeOH-*d*₄): δ 7.97 (s, 1H), 7.45 (d, *J* = 7.7 Hz, 1H), 7.22 (d, *J* = 7.8 Hz, 1H), 6.86–6.90 (m, 2H), 4.47 (t, *J* = 6.6 Hz, 2H), 3.87 (s, 3H), 2.21–2.26 (m, 4H), 2.05–2.07 (m, 1H). ¹³C NMR (100 MHz, CDCl₃/MeOH-*d*₄): δ 157.7, 152.6, 141.8, 132.5, 128.3, 121.1, 111.1, 81.6, 70.5, 55.9, 49.0, 27.0, 15.3. MS (ESI): m/z 340.0 [M + H]⁺. HRMS (ESI): m/z [M + H]⁺ calcd for C₁₇H₁₈N₅OS 340.1232, found 340.1218. HPLC: (a) t_R = 7.70 min, 98.8%; (b) t_R = 6.44 min, 99.1%.

(2-(6-Amino-3-(pent-4-ynyl)-3H-purin-8-ylthio)phenyl)methanol (9c'). Yield: 21%. ¹H NMR (400 MHz, CDCl₃/MeOH-*d*₄): δ 7.96 (s, 1H), 7.74 (d, *J* = 7.6 Hz, 1H), 7.60 (d, *J* = 7.5 Hz, 1H), 7.44 (t, *J* = 7.4 Hz, 1H), 7.29 (t, *J* = 7.5 Hz, 1H), 4.92 (s, 2H), 4.40 (t, *J* = 6.4 Hz, 2H), 3.47 (br s, 1H), 2.11–2.20 (m, 4H), 2.03–2.06 (m, 1H). ¹³C NMR (100 MHz, CDCl₃/MeOH-*d*₄): δ 146.2, 142.6, 137.3, 131.5, 130.9, 129.1, 82.1, 71.2, 64.9, 49.6, 27.1, 15.6. MS (ESI): m/z 340.1 [M + H]⁺. HRMS (ESI): m/z [M + H]⁺ calcd for C₁₇H₁₈N₅OS 340.1232, found 340.1242. HPLC: (a) t_R = 7.07 min, 98.9%; (b) t_R = 5.40 min, 99.0%.

3-(Pent-4-ynyl)-8-(2-(trifluoromethoxy)phenylthio)-3H-purin-6-amine (9d'). Yield: 19%. ¹H NMR (400 MHz, CDCl₃/MeOH-*d*₄): δ 8.01 (s, 1H), 7.50 (d, *J* = 7.9 Hz, 1H), 7.21–7.27 (m, 2H), 7.13 (t, *J* = 7.1 Hz, 1H), 4.48 (t, *J* = 6.1 Hz, 2H), 2.17–2.20 (m, 4H), 2.04–2.05 (m, 1H). ¹³C NMR (100 MHz, CDCl₃/MeOH-*d*₄): δ 158.3, 153.1, 142.2, 132.1, 128.1, 127.9, 126.9, 122.5, 120.7, 81.8, 70.5, 49.0, 26.9, 15.2. MS (ESI): m/z 393.7 [M + H]⁺. HRMS (ESI): m/z [M + H]⁺ calcd for C₁₇H₁₅N₅F₃OS 394.0949, found 394.0946. HPLC: (a) t_R = 8.82 min, 99.7%; (b) t_R = 7.19 min, 99.4%.

8-(2,4-Dichlorophenylthio)-3-(pent-4-ynyl)-3H-purin-6-amine (9g'). Yield: 22%. ¹H NMR (400 MHz, CDCl₃/MeOH-*d*₄): δ 8.10 (s, 1H), 7.50 (s, 1H), 7.42 (d, *J* = 8.4 Hz, 1H), 7.23–7.25 (m, 1H), 4.46 (t, *J* = 6.5 Hz, 2H), 2.24–2.27 (m, 2H), 2.14–2.19 (m, 3H). ¹³C NMR (100 MHz, CDCl₃/MeOH-*d*₄): δ 154.8, 152.9, 150.0, 142.8, 133.9, 132.3, 130.6, 129.3, 128.8, 127.2, 120.4, 81.3, 70.0, 49.8, 26.7, 14.7. MS (ESI): m/z 377.7 [M + H]⁺. HRMS (ESI): m/z [M + H]⁺ calcd for C₁₆H₁₄N₅Cl₂S 378.0347, found 378.0335. HPLC: (a) t_R = 9.18 min, 98.4%; (b) t_R = 7.35 min, 99.0%.

8-(2,4-Dimethylphenylthio)-3-(pent-4-ynyl)-3H-purin-6-amine (9i'). Yield: 27%. ¹H NMR (400 MHz, CDCl₃/MeOH-*d*₄): δ 7.94 (s, 1H), 7.48 (d, *J* = 7.7 Hz, 1H), 7.08 (s, 1H), 6.97 (d, *J* = 7.7 Hz, 1H), 4.36 (t, *J* = 6.1 Hz, 2H), 2.51 (s, 3H), 2.39 (s, 3H), 2.15–2.19 (m, 4H), 2.03–2.05 (m, 1H). ¹³C NMR (100 MHz, CDCl₃/MeOH-*d*₄): δ 162.6, 151.9, 151.1, 141.5, 141.1, 138.6, 134.5, 131.3, 127.3, 127.2, 121.7, 81.8, 70.5, 48.8, 26.9, 21.1, 20.8, 15.2. MS (ESI): m/z 338.1 [M + H]⁺. HRMS (ESI): m/z [M + H]⁺ calcd for C₁₈H₂₀N₅S 338.1439, found 338.1427. HPLC: (a) t_R = 8.24 min, 99.4%; (b) t_R = 7.19 min, 99.6%.

8-(2,4-Dimethoxyphenylthio)-3-(pent-4-ynyl)-3H-purin-6-amine (9j'). Yield: 7%. ¹H NMR (400 MHz, CDCl₃/MeOH-*d*₄): δ 7.99 (s, 1H), 7.53 (d, *J* = 8.1 Hz, 1H), 6.56–6.59 (m, 2H), 4.43 (t, *J* = 6.8 Hz, 2H), 3.86 (s, 3H), 3.82 (s, 3H), 2.12–2.26 (m, 5H). ¹³C NMR (100 MHz, CDCl₃/MeOH-*d*₄): δ 162.2, 160.6, 151.8, 141.6, 137.3, 135.2, 108.8, 105.3, 99.1, 81.5, 70.1, 55.6, 55.1, 26.7, 14.8. MS (ESI): m/z 370.0 [M + H]⁺. HRMS (ESI): m/z [M + H]⁺ calcd for C₁₈H₂₀N₅O₂S 370.1338, found 370.1350. HPLC: (a) t_R = 7.79 min, 97.9%; (b) t_R = 6.73 min, 98.7%.

8-(2,5-Dichlorophenylthio)-3-(pent-4-ynyl)-3H-purin-6-amine (9k'). Yield: 21%. ¹H NMR (400 MHz, CDCl₃/MeOH-*d*₄): δ 8.06 (s, 1H), 7.43 (s, 1H), 7.26–7.28 (m, 1H), 7.06–7.08 (m, 1H), 4.50–4.52 (m, 2H), 2.21–2.24 (m, 4H), 2.05–2.06 (m, 1H). ¹³C NMR (100 MHz, CDCl₃/MeOH-*d*₄): δ 153.6, 142.6, 132.7, 130.3, 129.7, 127.3, 81.7, 70.6, 49.2, 26.9, 15.2. MS (ESI): m/z 377.8 [M + H]⁺. HRMS (ESI): m/z [M + H]⁺ calcd for C₁₆H₁₄N₅Cl₂S 378.0347, found 378.0362. HPLC: (a) t_R = 9.07 min, 95.6%; (b) t_R = 7.30 min, 97.8%.

8-(2,5-Dimethylphenylthio)-3-(pent-4-ynyl)-3H-purin-6-amine (9l'). Yield: 20%. ¹H NMR (400 MHz, CDCl₃/MeOH-*d*₄): δ 7.96 (s, 1H), 7.41 (s, 1H), 7.13 (d, *J* = 7.7 Hz, 1H), 7.04 (d, *J* = 7.7 Hz, 1H),

4.45 (t, *J* = 6.3 Hz, 2H), 2.43 (s, 3H), 2.37 (s, 3H), 2.17–2.27 (m, 3H), 2.04 (m, 2H). ¹³C NMR (100 MHz, CDCl₃/MeOH-*d*₄): δ 152.0, 151.2, 141.7, 137.7, 135.9, 134.5, 130.9, 130.2, 129.2, 81.8, 70.5, 48.9, 27.0, 20.8, 20.4, 15.3. HRMS (ESI): m/z [M + H]⁺ calcd for C₁₈H₂₀N₅S 338.1439, found 338.1435. HPLC: (a) t_R = 8.67 min, 95.7%.

8-(2-Chloro-5-(trifluoromethyl)phenylthio)-3-(pent-4-ynyl)-3H-purin-6-amine (9m'). Yield: 18%. ¹H NMR (400 MHz, CDCl₃/MeOH-*d*₄): δ 8.08 (s, 1H), 7.84 (s, 1H), 7.57 (d, *J* = 8.3 Hz, 1H), 7.47 (d, *J* = 8.4 Hz, 1H), 4.48 (t, *J* = 6.5 Hz, 2H), 2.16–2.26 (m, 4H), 2.09–2.10 (m, 1H). ¹³C NMR (100 MHz, CDCl₃/MeOH-*d*₄): δ 157.4, 153.2, 150.4, 142.8, 138.2, 134.5, 130.1, 129.4, 128.9, 124.8, 121.9, 81.5, 70.4, 28.3, 26.7, 15.0. MS (ESI): m/z 411.8 [M + H]⁺. HPLC: (a) t_R = 9.38 min, 95.0%; (b) t_R = 7.66 min, 97.5%.

8-(3,5-Dichlorophenylthio)-3-(pent-4-ynyl)-3H-purin-6-amine (9n'). Yield: 14%. ¹H NMR (400 MHz, CDCl₃/MeOH-*d*₄): δ 8.03 (s, 1H), 7.46 (s, 2H), 7.30 (s, 1H), 4.50–4.52 (m, 2H), 2.20–2.24 (m, 3H), 2.04–2.07 (m, 2H). ¹³C NMR (100 MHz, CDCl₃/MeOH-*d*₄): δ 157.6, 152.6, 150.8, 142.9, 136.3, 134.8, 128.7, 127.1, 120.4, 81.3, 70.1, 43.8, 26.7, 14.7. MS (ESI): m/z 377.8 [M + H]⁺. HRMS (ESI): m/z [M + H]⁺ calcd for C₁₆H₁₃N₅Cl₂S 378.0347, found 378.0340. HPLC: (a) t_R = 9.50 min, 99.3%; (b) t_R = 7.57 min, 99.5%.

8-(3-Bromo-5-chlorophenylthio)-9-(pent-4-yn-1-yl)-9H-purin-6-amine (9o). Yield: 37%. ¹H NMR (400 MHz, CDCl₃): δ 8.36 (1H, s), 7.42–7.44 (2H, m), 7.33 (1H, s), 6.19 (2H, br s), 4.33 (2H, t, *J* = 7.3 Hz), 2.27 (2H, td, *J* = 6.6, 2.4 Hz), 1.99–2.03 (3H, m). ¹³C NMR (CDCl₃): δ 154.9, 153.5, 151.5, 143.5, 135.9, 134.7, 131.2, 131.0, 128.7, 123.4, 120.3, 82.3, 69.7, 43.0, 28.3, 16.0. HRMS (ESI): m/z [M + H]⁺ calcd for C₁₆H₁₄N₅SClBr 423.9821, found 423.9822.

8-((3,5-Dibromophenylthio)-9-(pent-4-yn-1-yl)-9H-purin-6-amine (9p). Yield: 37%. ¹H NMR (400 MHz, CDCl₃): δ 8.31 (1H, s), 7.62 (1H, t, *J* = 1.6 Hz), 7.50 (2H, d, *J* = 1.7 Hz), 6.22 (2H, br s), 4.33 (2H, t, *J* = 7.5 Hz), 2.27 (2H, td, *J* = 6.8, 2.6 Hz), 1.99–2.05 (3H, m). ¹³C NMR (CDCl₃): δ 154.2, 152.9, 151.6, 145.8, 134.1, 131.8, 128.2, 123.6, 114.5, 82.4, 69.7, 43.0, 28.2, 16.0. HRMS (ESI): m/z [M + H]⁺ calcd for C₁₆H₁₄N₅SBr₂ 465.9337, found 465.9329.

8-(3,5-Dimethylphenylthio)-3-(pent-4-ynyl)-3H-purin-6-amine (9q'). Yield: 16%. ¹H NMR (400 MHz, CDCl₃/MeOH-*d*₄): δ 8.01 (s, 1H), 7.23 (s, 2H), 7.00 (s, 1H), 4.45 (t, *J* = 7.5 Hz, 2H), 2.26 (s, 6H), 2.21–2.25 (m, 4H), 1.94–1.99 (m, 1H). MS (ESI): m/z 338.1 [M + H]⁺. HRMS (ESI): m/z [M + H]⁺ calcd for C₁₈H₂₀N₅S 338.1439, found 338.1426. HPLC: (a) t_R = 8.80 min, 98.9%; (b) t_R = 7.36 min, 99.2%.

8-((2,6-Dichloropyridin-4-ylthio)-9-(pent-4-yn-1-yl)-9H-purin-6-amine (9r). Yield: 22%. ¹H NMR (600 MHz, CDCl₃/MeOH-*d*₄): δ 8.32 (s, 1H), 7.47 (s, 1H), 7.18 (s, 1H), 4.38 (t, *J* = 7.2 Hz, 2H), 2.26–2.29 (m, 2H), 2.03–2.05 (m, 3H). ¹³C NMR (150 MHz, CDCl₃/MeOH-*d*₄): δ 159.3, 157.6, 155.0, 154.9, 153.9, 124.4, 124.3, 85.8, 73.6, 47.3, 41.7, 32.3, 19.7. HRMS (ESI): m/z [M + H]⁺ calcd for C₁₅H₁₃N₆SCl₂ 379.0299, found 379.0312.

8-((3,4-Dichlorophenylthio)-9-(pent-4-yn-1-yl)-9H-purin-6-amine (9t). Yield: 54%. ¹H NMR (400 MHz, CDCl₃): δ 8.25 (1H, s), 7.58 (1H, d, *J* = 2.2 Hz), 7.40 (1H, d, *J* = 8.4 Hz), 7.25 (1H, dd, *J* = 8.3, 2.1 Hz), 6.97 (2H, br s), 4.32 (2H, t, *J* = 7.4 Hz), 2.28 (2H, td, *J* = 6.8, 2.6 Hz), 1.97–2.02 (3H, m). ¹³C NMR (CDCl₃): δ 154.8, 153.3, 151.5, 144.6, 133.6, 133.0, 132.5, 131.3, 130.6, 130.2, 120.1, 82.3, 69.6, 42.9, 28.2, 16.0. MS (ESI): m/z 378.9 [M + H]⁺. HPLC: t_R = 8.50 min. HRMS (ESI): m/z [M + H]⁺ calcd for C₁₆H₁₄N₅SCl₂ 378.0347, found 378.0353.

9-(Pent-4-yn-1-yl)-8-((2,3,4-trichlorophenylthio)-9H-purin-6-amine (9u). Yield: 39%. ¹H NMR (400 MHz, CDCl₃): δ 8.35 (1H, s), 7.29 (1H, d, *J* = 8.6 Hz), 6.97 (1H, d, *J* = 8.6 Hz), 6.18 (2H, br s), 4.34 (2H, t, *J* = 7.3 Hz), 2.26 (2H, td, *J* = 6.8, 2.4 Hz), 2.03 (2H, p, *J* = 6.9 Hz), 1.98 (1H, t, *J* = 2.5 Hz). ¹³C NMR (CDCl₃): δ 154.8, 153.6, 151.5, 143.2, 133.5, 133.4, 133.0, 132.4, 128.8, 128.4, 120.5, 82.1, 69.7, 43.1, 28.4, 16.0. MS (ESI): m/z 412.0 [M + H]⁺. HPLC: t_R = 8.78 min. HRMS (ESI): m/z [M + H]⁺ calcd for C₁₆H₁₃N₅SCl₃ 411.9957, found 411.9967.

3-(Pent-4-ynyl)-8-(2,4,5-trichlorophenylthio)-3H-purin-6-amine (9v'). Yield: 23%. ¹H NMR (400 MHz, CDCl₃/MeOH-*d*₄): δ 8.04 (s, 1H), 7.73 (s, 1H), 7.55 (s, 1H), 4.50 (t, *J* = 6.4 Hz, 2H), 2.08–2.29

(m, 4H), 2.06–2.07 (m, 1H). ¹³C NMR (100 MHz, CDCl₃/MeOH-*d*₄): δ 159.6, 154.7, 152.4, 144.3, 135.3, 134.9, 134.7, 133.5, 132.9, 132.4, 128.8, 83.4, 72.2, 48.6, 28.6, 16.8. MS (ESI): *m/z* [M + H]⁺. HRMS (ESI): *m/z* [M + H]⁺ calcd for C₁₆H₁₃N₅Cl₃S 411.9957, found 411.9947. HPLC: (a) *t*_R = 9.84 min, 99.5%; (b) *t*_R = 7.96 min, 99.4%.

8-(Mesitylthio)-9-(pent-4-yn-1-yl)-9H-purin-6-amine (9w). Yield: 32%. ¹H NMR (400 MHz, CDCl₃): δ 8.21 (s, 1H), 6.98 (s, 2H), 5.87 (br s, 2H), 4.31 (t, 2H), 2.40 (s, 6H), 2.29–2.34 (m, 2H), 2.23 (s, 3H), 2.12 (m, 2H), 2.01 (m, 1H). ¹³C NMR (100 MHz, CDCl₃): δ 153.7, 151.8, 151.7, 143.3, 140.2, 129.5, 123.1, 119.7, 82.5, 69.4, 49.9, 42.4, 28.2, 21.8, 21.0, 16.1. MS (ESI): *m/z* [M + H]⁺. HRMS (ESI): *m/z* [M + H]⁺ calcd for C₁₉H₂₂N₅S 352.1596, found 352.1598. HPLC: (a) *t*_R = 6.58 min, 99.6%.

8-(Mesitylthio)-3-(pent-4-ynyl)-3H-purin-6-amine (9w'). Yield: 15%. ¹H NMR (400 MHz, CDCl₃/MeOH-*d*₄): δ 7.93 (s, 1H), 6.97 (s, 2H), 4.38 (t, *J* = 6.5 Hz, 2H), 2.41 (s, 6H), 2.30 (s, 3H), 2.04–2.16 (m, 5H). ¹³C NMR (100 MHz, CDCl₃/MeOH-*d*₄): δ 157.4, 150.4, 143.0, 142.2, 139.2, 128.9, 124.8, 81.5, 70.1, 26.7, 21.6, 21.3, 20.5, 14.8. MS (ESI): *m/z* [M + H]⁺. HRMS (ESI): *m/z* [M + H]⁺ calcd for C₁₉H₂₂N₅S 352.1596, found 352.1594. HPLC: (a) *t*_R = 9.05 min, 99.6%; (b) *t*_R = 7.49 min, 99.7%.

Formation of **9a–n**, **9q**, and **9v** followed a similar protocol. Synthesis and characterization of these coupling products have been described elsewhere.²⁴

8-Bromo-9H-purin-6-amine (11). Adenine (2.2 g, 16.3 mmol) was added to a solution of bromine (6.0 mL, 117.7 mmol) in water (200 mL), and the resulting mixture was stirred overnight at room temperature. The solvent was evaporated to dryness to yield **11**, which was used further without additional purification. MS (ESI): *m/z* 213.5/215.6 [M + H]⁺.

8-Bromo-9-(pent-4-yn-1-yl)-9H-purin-6-amine (12). A mixture of 8-bromo-adenine (**11**; 0.1 g, 0.47 mmol), Cs₂CO₃ (0.3 g, 0.94 mmol), and 5-chloropent-1-yne (0.13g, 0.65 mmol) in DMF (1.5 mL) under nitrogen protection was heated at 80 °C for 2 h. Following solvent removal, the crude material was purified by preparatory TLC with CH₂Cl₂:MeOH:AcOH at 20:1:0.1 to provide 36 mg (30%) of **12**. ¹H NMR (500 MHz, CDCl₃/MeOH-*d*₄): δ 8.29 (s, 1H), 4.33 (t, *J* = 7.2 Hz, 2H), 2.28–2.33 (m, 2H), 2.09 (q, *J* = 7.0 Hz, 2H), 2.01–2.03 (t, 1H). ¹³C NMR (125 MHz, CDCl₃/MeOH-*d*₄): δ 154.4, 153.1, 151.3, 127.4, 119.9, 82.4, 69.7, 43.8, 28.2, 16.1. MS (ESI): *m/z* 280.1/282.2 [M + H]⁺.

5-((6-Amino-9-(pent-4-yn-1-yl)-9H-purin-8-yl)thio)-isophthalonitrile (9s). A mixture of 5-mercaptoisophthalonitrile²⁶ (11 mg, 0.069 mmol) and *t*-BuOK (7 mg, 0.069 mmol) in 1.5 mL of DMF was stirred for 15 min at room temperature. Compound **12** (16 mg, 0.057 mmol) was then added and the reaction mixture was allowed to stir at 80 °C for 2 h. Following solvent removal, the crude material was purified by preparatory TLC with CH₂Cl₂:MeOH at 20:1 to provide 10.2 mg (51%) of the title compound. ¹H NMR (600 MHz, CDCl₃/MeOH-*d*₄): δ 8.38 (s, 1H), 7.98 (s, 2H), 7.85 (s, 1H), 4.37 (t, *J* = 7.3 Hz, 2H), 2.27–2.30 (m, 2H), 2.05 (q, *J* = 6.9 Hz, 2H), 2.01–2.03 (t, 1H). ¹³C NMR (150 MHz, CDCl₃/MeOH-*d*₄): δ 154.7, 153.8, 151.7, 142.2, 136.9, 136.1, 134.3, 120.5, 115.8, 115.2, 82.2, 69.8, 43.1, 28.3, 15.9. HRMS (ESI): *m/z* [M + H]⁺ calcd for C₁₈H₁₄N₇S 360.1031, found 360.1028.

General Procedure for the Synthesis of 13a–k,m,o,q,r. A mixture of 8-((3,5-dichlorophenyl)thio)-9H-purin-6-amine (1.0 mmol), Cs₂CO₃ (1.2 mmol), and the respective alkyl bromides or alkyl benzenesulfonate (2.0 mmol) in DMF (1.5 mL) under nitrogen atmosphere was heated at 80 °C for 30 min. Following solvent removal, the crude material was purified by preparatory TLC with CHCl₃:MeOH:NH₄OH at 10:1:0.5 or CHCl₃:MeOH:AcOH at 10:1:0.5 to provide the corresponding 9-alkyl-8-arylsulfanyladenine derivatives.

9-(But-3-yn-1-yl)-8-((3,5-dichlorophenyl)thio)-9H-purin-6-amine (13a). Yield: 47%. ¹H NMR (400 MHz, CDCl₃): δ 8.37 (1H, s), 7.28 (3H, s), 6.04 (2H, br s), 4.45 (2H, t, *J* = 7.0 Hz), 2.76 (2H, td, *J* = 6.8, 2.3 Hz), 1.95 (1H, t, *J* = 2.4 Hz). ¹³C NMR (CDCl₃): δ 154.9, 153.6, 151.3, 143.7, 135.8, 134.9, 128.3, 127.9, 120.4, 79.4, 71.5, 42.3, 19.5.

HRMS (ESI): *m/z* [M + H]⁺ calcd for C₁₅H₁₂N₅SCl₂ 364.0190, found 364.0194.

8-((3,5-Dichlorophenyl)thio)-9-(hex-5-yn-1-yl)-9H-purin-6-amine (13b). Yield: 41%. ¹H NMR (400 MHz, CDCl₃): δ 8.29 (1H, s), 7.28 (3H, s), 6.71 (2H, br s), 4.26 (2H, t, *J* = 7.2 Hz), 2.22 (2H, td, *J* = 6.8, 2.7 Hz), 1.95 (1H, t, *J* = 2.6 Hz), 1.87–1.93 (2H, m), 1.53 (2H, pentet, *J* = 6.8 Hz). ¹³C NMR (CDCl₃): δ 155.0, 151.2, 143.6, 135.9, 134.4, 129.0, 128.5, 128.2, 120.0, 83.3, 69.1, 43.5, 28.8, 25.3, 17.9. HRMS (ESI): *m/z* [M + H]⁺ calcd for C₁₇H₁₅N₅SCl₂ 392.0503, found 392.0493.

9-(But-2-yn-1-yl)-8-((3,5-dichlorophenyl)thio)-9H-purin-6-amine (13c). Yield: 40%. ¹H NMR (500 MHz, CDCl₃): δ 8.33 (1H, s), 7.32 (2H, s), 7.28 (1H, s), 6.63 (2H, br s), 4.98–4.99 (2H, m), 1.70 (3H, m). ¹³C NMR (CDCl₃): δ 155.1, 153.2, 150.8, 143.3, 135.7, 134.5, 128.5, 128.3, 120.0, 82.1, 71.7, 33.4, 3.5. HRMS (ESI): *m/z* [M + H]⁺ calcd for C₁₅H₁₂N₅SCl₂ 364.0190, found 364.0197.

8-((3,5-Dichlorophenyl)thio)-9-(3,3,3-trifluoropropyl)-9H-purin-6-amine (13d). Yield: 43%. ¹H NMR (400 MHz, CDCl₃): δ 8.33 (1H, s), 7.29 (3H, s), 6.44 (2H, br s), 4.49 (2H, t, *J* = 6.8 Hz), 2.64–2.68 (2H, m). ¹³C NMR (CDCl₃): δ 155.0, 153.4, 151.2, 143.5, 136.0, 133.8, 128.8, 128.4, 126.6, 120.2, 37.3, 33.3. HRMS (ESI): *m/z* [M + H]⁺ calcd for C₁₄H₁₁N₅SCl₂F₃ 408.0064, found 408.0074.

8-((3,5-Dichlorophenyl)thio)-9-(4,4,4-trifluorobutyl)-9H-purin-6-amine (13e). Yield: 44%. ¹H NMR (400 MHz, CDCl₃): δ 8.36 (1H, s), 7.28 (3H, s), 6.16 (2H, br s), 4.30 (2H, t, *J* = 6.6 Hz), 2.10–2.14 (2H, m), 2.03–2.05 (2H, m). ¹³C NMR (CDCl₃): δ 154.9, 153.7, 151.5, 143.2, 135.9, 134.2, 128.6, 128.1, 125.1, 120.3, 42.5, 31.3, 22.5. HRMS (ESI): *m/z* [M + H]⁺ calcd for C₁₅H₁₃N₅SCl₂F₃ 422.0221, found 422.0222.

8-((3,5-Dichlorophenyl)thio)-9-(5,5,5-trifluoropentyl)-9H-purin-6-amine (13f). Yield: 45%. ¹H NMR (400 MHz, CDCl₃): δ 8.28 (1H, s), 7.28 (3H, s), 6.82 (2H, br s), 4.25 (2H, t, *J* = 7.2 Hz), 2.07–2.14 (2H, m), 1.85 (2H, pentet, *J* = 7.4 Hz), 1.57 (2H, pentet, *J* = 7.5 Hz). ¹³C NMR (CDCl₃): δ 155.1, 152.7, 151.2, 143.5, 135.9, 134.1, 128.6, 128.2, 125.4, 120.1, 43.3, 33.1, 28.8, 19.2. HRMS (ESI): *m/z* [M + H]⁺ calcd for C₁₆H₁₅N₅SCl₂F₃ 436.0377, found 436.0363.

8-((3,5-Dichlorophenyl)thio)-9-(6,6,6-trifluorohexyl)-9H-purin-6-amine (13g). Yield: 47%. ¹H NMR (400 MHz, CDCl₃): δ 8.35 (1H, s), 7.29 (3H, s), 6.33 (2H, br s), 4.24 (2H, t, *J* = 7.2 Hz), 2.00–2.07 (2H, m), 1.79 (2H, pentet, *J* = 7.4 Hz), 1.57 (2H, pentet, *J* = 7.6 Hz), 1.37 (2H, pentet, *J* = 7.8 Hz). ¹³C NMR (CDCl₃): δ 155.1, 152.8, 151.3, 143.4, 135.9, 134.4, 128.5, 128.1, 125.8, 120.0, 43.6, 33.9, 29.4, 25.7, 21.4. HRMS (ESI): *m/z* [M + H]⁺ calcd for C₁₇H₁₇N₅SCl₂F₃ 450.0534, found 450.0549.

4-(6-Amino-8-((3,5-dichlorophenyl)thio)-9H-purin-9-yl)-butanenitrile (13h). Yield: 41%. ¹H NMR (400 MHz, CDCl₃): δ 8.34 (1H, s), 7.31 (3H, s), 6.04 (2H, br s), 4.36 (2H, t, *J* = 7.0 Hz), 2.42 (2H, t, *J* = 7.1 Hz), 2.18 (2H, pentet, *J* = 7.2 Hz). ¹³C NMR (CDCl₃): δ 154.8, 152.7, 151.5, 143.4, 136.0, 133.9, 129.2, 127.5, 120.2, 118.3, 42.4, 25.6, 14.9. HRMS (ESI): *m/z* [M + H]⁺ calcd for C₁₅H₁₃N₆SCl₂ 379.0299, found 379.0303.

9-Benzyl-8-((3,5-dichlorophenyl)thio)-9H-purin-6-amine (13i). Yield: 48%. ¹H NMR (400 MHz, CDCl₃): δ 8.43 (1H, s), 7.23 (3H, s), 7.15–7.19 (3H, m), 7.04–7.05 (2H, m), 5.97 (2H, br s), 5.45 (2H, s). ¹³C NMR (CDCl₃): δ 154.9, 153.9, 151.7, 143.6, 135.6, 135.3, 134.5, 128.7, 128.2, 128.1, 127.9, 127.5, 120.8, 47.0. HRMS (ESI): *m/z* [M + H]⁺ calcd for C₁₈H₁₄N₅SCl₂ 402.0347, found 402.0335.

8-((3,5-Dichlorophenyl)thio)-9-phenethyl-9H-purin-6-amine (13j). Yield: 45%. ¹H NMR (400 MHz, CDCl₃): δ 8.35 (1H, s), 7.22–7.26 (4H, m), 7.19–7.20 (2H, m), 7.04–7.06 (2H, m), 6.45 (2H, br s), 4.47 (2H, t, *J* = 7.2 Hz), 3.09 (2H, t, *J* = 7.3 Hz). ¹³C NMR (CDCl₃): δ 153.8, 151.5, 151.2, 145.1, 136.8, 135.8, 134.0, 128.9, 128.8, 128.6, 128.5, 127.2, 120.1, 45.5, 35.7. HRMS (ESI): *m/z* [M + H]⁺ calcd for C₁₉H₁₆N₅SCl₂ 416.0503, found 416.0508.

8-((3,5-Dichlorophenyl)thio)-9-(pent-4-yn-2-yl)-9H-purin-6-amine (13m). Yield: 12%. ¹H NMR (600 MHz, CDCl₃): δ 8.27 (s, 1H), 7.26–7.28 (m, 3H), 6.28 (br s, 2H), 4.96 (m, 1H), 3.31 (ddd, *J* = 2.6, 9.6, 16.9 Hz, 1H), 2.82 (ddd, *J* = 2.6, 5.9, 16.9 Hz, 1H), 1.83 (t, *J* = 2.6 Hz, 1H), 1.66 (d, *J* = 6.9 Hz, 3H). ¹³C NMR (150 MHz, CDCl₃): δ 155.0, 152.4, 151.1, 143.6, 135.8, 135.3, 128.2, 127.9, 120.6, 80.0,

70.8, 53.4, 24.9, 19.3. HRMS (ESI): m/z [M + H]⁺ calcd for C₁₆H₁₄N₅SCl₂ 378.0347, found 378.0336.

9-Butyl-8-((2,4-dichlorophenyl)thio)-9H-purin-6-amine (13o). Yield: 23%. ¹H NMR (600 MHz, CDCl₃): δ 8.36 (s, 1H), 7.47 (d, J = 2.1 Hz, 1H), 7.17–7.19 (m, 1H), 7.13–7.15 (m, 1H), 5.71 (br s, 2H), 4.22 (t, J = 7.5 Hz, 2H), 1.72–1.77 (m, 2H), 1.32–1.36 (m, 2H), 0.92 (t, J = 7.3 Hz, 3H). ¹³C NMR (150 MHz, CDCl₃): δ 154.6, 153.4, 151.6, 143.8, 134.9, 134.6, 132.3, 130.1, 129.9, 128.1, 120.4, 43.8, 31.4, 19.9, 13.5. HRMS (ESI): m/z [M + H]⁺ calcd for C₁₅H₁₆N₅SCl₂ 368.0503, found 368.0493.

9-(But-3-yn-1-yl)-8-((2,4-dichlorophenyl)thio)-9H-purin-6-amine (13q). Yield: 20%. ¹H NMR (600 MHz, CDCl₃): δ 8.33 (s, 1H), 7.47 (s, 1H), 7.21 (m, 2H), 5.96 (br s, 2H), 4.45 (t, J = 7.0 Hz, 2H), 2.75–2.78 (m, 2H), 1.95 (t, J = 2.5 Hz, 1H). ¹³C NMR (150 MHz, CDCl₃): δ 154.6, 153.1, 151.3, 144.4, 135.2, 134.8, 132.6, 130.2, 129.8, 128.1, 120.3, 79.3, 71.5, 42.3, 19.6. HRMS (ESI): m/z [M + H]⁺ calcd for C₁₅H₁₂N₅SCl₂ 364.0190, found 364.0177.

8-((2,4-Dichlorophenyl)thio)-9-(pent-4-yn-2-yl)-9H-purin-6-amine (13r). Yield: 12%. ¹H NMR (600 MHz, CDCl₃): δ 8.27 (s, 1H), 7.47 (d, J = 2.0 Hz, 1H), 7.14–7.18 (m, 2H), 6.13 (br s, 2H), 4.98 (m, 1H), 3.31 (ddd, J = 2.6, 9.2, 16.9 Hz, 1H), 2.82 (ddd, J = 2.6, 6.2, 16.9 Hz, 1H), 1.83 (t, J = 2.6 Hz, 1H), 1.66 (d, J = 6.9 Hz, 3H). ¹³C NMR (150 MHz, CDCl₃): δ 154.8, 152.3, 151.2, 144.1, 134.8, 134.5, 132.3, 130.2, 130.0, 127.9, 120.7, 80.0, 70.8, 53.4, 24.5, 19.1. HRMS (ESI): m/z [M + H]⁺ calcd for C₁₆H₁₄N₅SCl₂ 378.0347, found 378.0354.

General Procedure for the Synthesis of 13l,n,p,s. To a suspension of 8-((2,4-dichlorophenyl)thio)-9H-purin-6-amine (1.0 mmol) in CH₂Cl₂:toluene (0.5:2.5 mL) were added PPh₃ (4.0 mmol) and alcohol (2.0 mmol) under nitrogen protection. After stirring for 10 min, DBAD (6 mmol) was added and the reaction mixture was stirred at rt for 2–5 h. Following solvent removal, the crude material was purified by preparative TLC [CH₂Cl₂:CH₃OH:AcOH, 20:1:0.1 or CH₂Cl₂:NH₃–CH₃OH (7 N), 20:1] to afford the desired compounds.

8-((3,5-Dichlorophenyl)thio)-9-(pentan-2-yl)-9H-purin-6-amine (13l). Yield: 15%. ¹H NMR (600 MHz, CDCl₃/MeOH-*d*₄, two rotamers): δ 8.17–8.21 (m, 1H), 7.40–7.56 (m, 3H), 4.76–4.79 (m, 0.4H), 4.65–4.69 (m, 0.6H), 2.21–2.27 (m, 0.6H), 1.97–2.03 (m, 0.4H), 1.81–1.92 (m, 1H), 1.60–1.63 (m, 3H), 1.03–1.28 (m, 2H), 0.87–0.89 (m, 3H). ¹³C NMR (150 MHz, CDCl₃/MeOH-*d*₄): δ 153.3, 151.2, 150.0, 145.6, 135.9, 135.2, 133.5, 130.2, 129.1, 128.1, 120.4, 54.4, 36.7, 19.8, 19.7, 13.6. HRMS (ESI): m/z [M + H]⁺ calcd for C₁₆H₁₈Cl₂N₅S 382.0660, found 382.0663.

8-((3,5-Dichlorophenyl)thio)-9-(hex-5-yn-3-yl)-9H-purin-6-amine (13n). Yield: 37%. ¹H NMR (600 MHz, CDCl₃): δ 8.25 (s, 1H), 7.35–7.37 (m, 2H), 7.33 (t, J = 1.7 Hz, 1H), 4.71–4.74 (m, 1H), 3.27–3.33 (m, 1H), 2.80–2.84 (m, 1H), 2.32–2.35 (m, 1H), 2.02–2.05 (m, 1H), 1.84 (t, J = 2.5 Hz, 1H), 0.79 (t, J = 7.4 Hz, 3H). ¹³C NMR (150 MHz, CDCl₃): δ 153.6, 150.5, 147.7, 135.8, 133.6, 132.1, 131.9, 129.3, 128.9, 128.4, 79.6, 71.1, 59.9, 26.2, 23.3, 10.9. HRMS (ESI): m/z [M + H]⁺ calcd for C₁₇H₁₅Cl₂N₅S 392.0503, found 392.0503.

8-((2,4-Dichlorophenyl)thio)-9-(pentan-2-yl)-9H-purin-6-amine (13p). Yield: 15%. ¹H NMR (600 MHz, CDCl₃): δ 8.22 (s, 1H), 7.43 (d, J = 1.8 Hz, 1H), 7.13–7.20 (m, 2H), 6.14 (br s, 2H), 4.65–4.70 (m, 1H), 2.17–2.23 (m, 1H), 1.80–1.86 (m, 1H), 1.54 (d, J = 6.9 Hz, 3H), 1.12–1.19 (m, 1H), 0.97–1.02 (m, 1H), 0.79 (t, J = 7.4 Hz, 3H). ¹³C NMR (150 MHz, CDCl₃): δ 153.3, 151.2, 150.0, 145.6, 135.9, 135.2, 133.5, 130.2, 129.1, 128.1, 120.4, 54.4, 36.7, 19.8, 19.7, 13.6. HRMS (ESI): m/z [M + H]⁺ calcd for C₁₆H₁₈Cl₂N₅S 382.0660, found 382.0663.

8-((2,4-Dichlorophenyl)thio)-9-(hex-5-yn-3-yl)-9H-purin-6-amine (13s). Yield: 24%. ¹H NMR (600 MHz, MeOH-*d*₄): δ 8.27 (s, 1H), 7.69 (d, J = 2.2 Hz, 1H), 7.63 (d, J = 8.5 Hz, 1H), 7.42 (d, J = 8.5 and 2.3 Hz, 1H), 4.75–4.79 (m, 1H), 3.24–3.28 (m, 1H), 2.89–2.94 (m, 1H), 2.35–2.41 (m, 1H), 2.25 (t, J = 2.6 Hz, 1H), 2.05–2.10 (m, 1H), 0.84 (t, J = 7.4 Hz, 3H). ¹³C NMR (150 MHz, MeOH-*d*₄): δ 153.3, 151.2, 150.0, 145.6, 135.9, 135.2, 133.5, 130.2, 129.1, 128.1, 120.4, 54.4, 36.7, 19.8, 19.7, 13.6. HRMS (ESI): m/z [M + H]⁺ calcd for C₁₇H₁₆Cl₂N₅S 392.0660, found 392.0663.

Synthesis of 14a and 14b. A mixture of 9g (20 mg, 0.053 mmol) and *m*-CPBA (18.2 mg, 0.106 mmol) in THF:CH₂Cl₂ (2 mL) under nitrogen protection was stirred at room temperature for 30 min. Following solvent removal, the crude material was purified by preparative TLC [CH₂Cl₂:CH₃OH–NH₃ (7 N), 20:1] to afford 14a and 14b.

8-((2,4-Dichlorophenyl)sulfonyl)-9-(pent-4-yn-1-yl)-9H-purin-6-amine (14a). Yield: 23%. ¹H NMR (600 MHz, CDCl₃/MeOH-*d*₄): δ 8.29 (s, 1H), 8.04 (d, J = 8.5 Hz, 1H), 7.58 (dd, J = 8.5, 2.0 Hz, 1H), 7.41 (d, J = 2.0 Hz, 1H), 4.57 (t, J = 7.1 Hz, 2H), 2.30 (td, J = 7.0, 2.6 Hz, 2H), 2.06–2.20 (m, 2H), 1.98 (t, J = 2.6 Hz, 1H). ¹³C NMR (150 MHz, CDCl₃/MeOH-*d*₄): δ 155.1, 152.6, 150.6, 139.2, 136.3, 131.9, 130.1, 128.7, 128.6, 119.1, 81.9, 70.0, 43.5, 28.7, 16.0. HRMS (ESI): m/z [M + H]⁺ calcd for C₁₆H₁₄Cl₂N₅OS 394.0296, found 394.0279.

8-((2,4-Dichlorophenyl)sulfonyl)-9-(pent-4-yn-1-yl)-9H-purin-6-amine (14b). Yield: 34%. ¹H NMR (600 MHz, CDCl₃): δ 8.39 (s, 1H), 8.24 (d, J = 8.4 Hz, 1H), 7.48–7.51 (m, 2H), 6.24 (br s, 2H), 4.88 (t, J = 7.6 Hz, 2H), 2.29 (td, J = 7.0, 2.6 Hz, 2H), 2.10–2.16 (m, 2H), 1.92 (t, J = 2.6 Hz, 1H). ¹³C NMR (150 MHz, CDCl₃): δ 155.4, 153.3, 150.7, 146.2, 142.2, 134.9, 134.8, 132.6, 132.0, 127.9, 119.3, 82.1, 69.6, 44.4, 28.9, 16.1. HRMS (ESI): m/z [M + H]⁺ calcd for C₁₆H₁₄Cl₂N₅O₂S 410.0245, found 410.0228.

8-(2,4-Dichlorophenoxy)-9-(pent-4-yn-1-yl)-9H-purin-6-amine (14c). A mixture of 2,4-dichlorophenol (0.069 mmol) and KO^tBu (0.069 mmol) in DMF (1.5 mL) was stirred for 15 min at room temperature. Compound 12 (0.057 mmol) was added and the reaction mixture was allowed to stir at 80 °C for 2 h. Following solvent removal, the crude material was purified by preparative TLC (CH₂Cl₂:MeOH, 20:1) to afford 14c. Yield: 51%. ¹H NMR (600 MHz, CDCl₃): δ 8.22 (s, 1H), 7.45 (d, J = 2.5 Hz, 1H), 7.43 (d, J = 8.7 Hz, 1H), 7.27 (dd, J = 8.7, 2.5 Hz, 1H), 5.42 (br s, 2H), 4.26 (t, J = 7.1 Hz, 2H), 2.27 (td, J = 7.0, 2.6 Hz, 2H), 2.09–2.14 (m, 2H), 1.90 (t, J = 2.6 Hz, 1H). ¹³C NMR (150 MHz, CDCl₃): δ 153.2, 152.7, 151.4, 149.9, 147.4, 132.1, 130.6, 128.9, 128.3, 127.1, 123.7, 115.4, 82.5, 69.4, 41.2, 27.9, 16.1. HRMS (ESI): m/z [M + H]⁺ calcd for C₁₆H₁₄Cl₂N₅O 362.0575, found 362.0570.

8-(2,4-Dichlorobenzyl)-9H-purin-6-amine (17). In a conical-bottomed Smith process vial, the mixture of 4,5,6-triaminopyrimidine (15, 0.21 g, 1.7 mmol), 2,4-dichlorophenylacetic acid (16; 0.25 g, 1.4 mmol), and triphenyl phosphite (0.52 g, 443 μL, 1.7 mmol) in 1.5 mL of anhydrous pyridine was charged. The sealed vial was irradiated in the microwave for 30 min at 220 °C. After cooling, the reaction mixture was concentrated under vacuum and the residue purified by column chromatography (CH₂Cl₂:MeOH, 10:0 to 10:1) to give the desired product 17. Yield: 79%. MS (ESI): m/z 294.0 [M + H]⁺.

8-(2,4-Dichlorobenzyl)-9-(pent-4-yn-1-yl)-9H-purin-6-amine (14d). A mixture of 17 (1.0 mmol), Cs₂CO₃ (1.2 mmol), and 1-chloro-pent-4-yne (2.0 mmol) in DMF (1.5 mL) under nitrogen protection was heated at 80 °C for 2 h. Following solvent removal, the crude material was purified by preparative TLC (CH₂Cl₂:MeOH:AcOH, 15:1:0.1) to provide 14d. Yield: 13%. ¹H NMR (600 MHz, CDCl₃): δ 8.25 (s, 1H), 7.38 (d, J = 2.2 Hz, 1H), 7.13 (dd, J = 8.3 and 2.2 Hz, 1H), 7.01 (d, J = 8.3 Hz, 1H), 5.86 (br s, 2H), 4.29 (s, 2H), 4.15 (t, J = 7.4 Hz, 2H), 2.17 (td, J = 6.8 and 2.6 Hz, 2H), 1.90–1.96 (m, 3H). ¹³C NMR (150 MHz, CDCl₃): δ 154.3, 151.7, 151.4, 150.2, 134.7, 134.1, 132.4, 131.4, 129.8, 127.8, 118.9, 82.5, 70.1, 42.3, 31.3, 28.4, 15.9. HRMS (ESI): m/z [M + H]⁺ calcd for C₁₇H₁₆Cl₂N₅ 360.0783, found 360.0772.

(6-Amino-9-(pent-4-yn-1-yl)-9H-purin-8-yl)(2,4-dichlorophenyl)methanone (14e). A mixture of 14d (1.0 mmol) and Cs₂CO₃ (2.0 mmol) in DMF (1.3 mL) was heated at 80 °C for 3 h. Following solvent removal, the crude material was purified by preparative TLC [CH₂Cl₂:CH₃OH–NH₃ (7 N), 20:1] to provide the corresponding aryl ketone 14e. Yield: 50%. ¹H NMR (600 MHz, CDCl₃): δ 8.25 (s, 1H), 7.49 (d, J = 8.2 Hz, 1H), 7.43 (d, J = 1.9 Hz, 1H), 7.33 (dd, J = 8.3, 1.9 Hz, 1H), 6.26 (br s, 2H), 4.73 (t, J = 7.2 Hz, 2H), 2.28 (td, J = 7.0, 2.6 Hz, 2H), 2.07–2.13 (m, 2H), 1.88 (t, J = 2.6 Hz, 1H). ¹³C NMR (150 MHz, CDCl₃): δ 185.5, 155.9, 153.5, 151.3, 144.4, 137.9, 135.5, 133.5, 131.4, 130.3, 127.1, 119.6, 82.4, 69.3, 44.1, 28.9, 16.1.

HRMS (ESI): m/z $[M + H]^+$ calcd for $C_{17}H_{14}Cl_2N_5O$ 374.0575, found 374.0571.

General Procedure for the Synthesis of 18a and 18b'. A mixture of 8-arylsulfanyladenine (100 mmol), Cs_2CO_3 (100 mmol), and 3-(*tert*-butoxycarbonyl-isopropyl-amino)propyl tosylate (200 mmol) in DMF (1.3 mL) under nitrogen protection was heated at 80 °C for 30 min. Following solvent removal, the crude material was purified by preparatory TLC with CH_2Cl_2 :MeOH:AcOH at 20:1:0.1 to afford the Boc-protected N9- and N3-alkylated compounds. They were separately treated with TFA (1 mL) at 0 °C for 1.5 h to provide with corresponding 9-alkyl-8-arylsulfanyladenine and 3-alkyl-8-arylsulfanyladenine derivatives.

8-((2,4-Dichlorophenyl)thio)-9-(3-(isopropylamino)propyl)-9H-purin-6-amine (18a). Yield: 35%. 1H NMR (600 MHz, $CDCl_3$ /MeOH- d_4): δ 8.23 (s, 1H), 7.55 (s, 1H), 7.38 (d, $J = 8.3$ Hz, 1H), 7.30 (d, $J = 8.3$ Hz, 1H), 4.34 (t, $J = 6.7$ Hz, 2H), 2.92 (septet, $J = 5.8$ Hz, 1H), 2.69 (t, $J = 6.4$ Hz, 2H), 2.13 (quintet, $J = 6.5$ Hz, 2H), 1.16 (d, $J = 5.7$ Hz, 6H). HRMS (ESI): m/z $[M + H]^+$ calcd for $C_{17}H_{21}Cl_2N_6S$ 411.0925, found 411.0907.

8-((2,4-Dimethylphenyl)thio)-3-(3-(isopropylamino)propyl)-3H-purin-6-amine (18b'). Yield: 29%. 1H NMR (500 MHz, $CDCl_3$): δ 7.96 (s, 1H), 7.48 (d, $J = 7.9$ Hz, 1H), 7.11 (s, 1H), 7.00 (d, $J = 7.8$ Hz, 1H), 4.48 (t, $J = 6.3$ Hz, 2H), 2.91 (septet, $J = 6.3$ Hz, 1H), 2.65 (t, $J = 6.1$ Hz, 2H), 2.25–2.29 (m, 2H), 1.18 (d, $J = 6.3$ Hz, 6H). HRMS (ESI): m/z $[M + H]^+$ calcd for $C_{19}H_{27}N_6S$ 371.2018, found 371.2035.

8-((3,5-Dichlorophenyl)thio)-9-(3-(isopropylamino)propyl)-9H-purin-6-amine (18c). Yield: 32%. 1H NMR (600 MHz, $CDCl_3$ /MeOH- d_4): δ 8.21 (s, 1H), 7.26 (t, $J = 1.7$ Hz, 1H), 7.24 (d, $J = 1.9$ Hz, 2H), 4.23 (t, $J = 6.9$ Hz, 2H), 2.63 (septet, $J = 6.2$ Hz, 1H), 2.46 (t, $J = 6.4$ Hz, 2H), 1.89 (quintet, $J = 6.9$ Hz, 2H), 0.97 (d, $J = 6.3$ Hz, 6H). ^{13}C NMR (150 MHz, $CDCl_3$): δ 154.7, 153.1, 151.3, 144.1, 135.9, 133.7, 128.8, 128.7, 119.7, 48.6, 43.4, 41.6, 29.8, 22.4. HRMS (ESI): m/z $[M + H]^+$ calcd for $C_{17}H_{21}Cl_2N_6S$ 411.0925, found 411.0917. HPLC: (a) $t_R = 6.28$ min, 99.5%.

8-((3,5-Dichlorophenyl)thio)-3-(3-(isopropylamino)propyl)-3H-purin-6-amine (18c'). Yield: 18%. 1H NMR (600 MHz, $CDCl_3$ /MeOH- d_4): δ 7.98 (s, 1H), 7.33 (d, $J = 1.8$ Hz, 2H), 7.06 (t, $J = 1.8$ Hz, 1H), 4.40 (t, $J = 6.7$ Hz, 2H), 2.66 (septet, $J = 6.2$ Hz, 1H), 2.51 (t, $J = 6.4$ Hz, 2H), 2.06 (quintet, $J = 6.5$ Hz, 2H), 0.96 (d, $J = 6.2$ Hz, 6H). ^{13}C NMR (150 MHz, $CDCl_3$): δ 157.9, 153.4, 151.0, 142.8, 137.8, 134.9, 127.9, 126.8, 122.6, 48.9, 48.1, 43.0, 29.5, 22.9. HRMS (ESI): m/z $[M + H]^+$ calcd for $C_{17}H_{21}Cl_2N_6S$ 411.0925, found 411.0928. HPLC: (a) $t_R = 4.95$ min, 99.7%.

General Procedure for the Synthesis of 20d–f. To 4-amino-1-(4-methoxybenzyl)-1H-imidazo[4,5-*c*]pyridine-2-thiol (**19**)²⁰ 50 mg, 0.174 mmol) were added the respective aryl iodide (0.348 mmol), neocuproine hydrate (3.6 mg, 0.0174 mmol), CuI (3.3 mg, 0.0174 mmol), sodium *tert*-butoxide (25 mg, 0.261 mmol), and DMF (5 mL), and the reaction mixture was stirred at 110 °C for 24 h. Then, the solvent was removed under reduced pressure and the crude product was purified by preparatory TLC [CH_2Cl_2 :MeOH–NH₃ (7 N), 10:1] to afford desired coupling derivatives **20d–f**.

2-((2,4-Dichlorophenyl)thio)-1-(4-methoxybenzyl)-1H-imidazo[4,5-*c*]pyridin-4-amine (20d). Yield: 40%. 1H NMR (500 MHz, $CDCl_3$ /MeOH- d_4): δ 7.78 (d, $J = 5.9$ Hz, 1H), 7.36 (d, $J = 2.1$ Hz, 1H), 7.02 (dd, $J = 8.5$, 2.1 Hz, 1H), 6.98 (d, $J = 8.6$ Hz, 2H), 6.91 (d, $J = 8.6$ Hz, 1H), 6.73 (d, $J = 8.6$ Hz, 2H), 6.65 (d, $J = 6.0$ Hz, 1H), 5.30 (s, 2H), 3.75 (s, 3H). MS (ESI): m/z 430.9 $[M + H]^+$.

2-((3,5-Dichlorophenyl)thio)-1-(4-methoxybenzyl)-1H-imidazo[4,5-*c*]pyridin-4-amine (20e). Yield: 39%. MS (ESI): m/z 431.0 $[M + H]^+$.

2-((6-Iodobenzo[d][1,3]dioxol-5-yl)thio)-1-(4-methoxybenzyl)-1H-imidazo[4,5-*c*]pyridin-4-amine (20f). Yield: 20%. MS (ESI): m/z 533.0 $[M + H]^+$.

General Procedure for the Synthesis of 21d–f. To coupling products **20d–f** (0.067 mmol) was added trifluoroacetic acid (3 mL), and the reaction mixture was stirred at 80 °C for 3 h. Then, the solvent was removed under reduced pressure and the crude product was

purified by preparatory TLC [CH_2Cl_2 :MeOH–NH₃ (7 N), 15:1] to afford corresponding deprotected intermediates **21d–f**.

2-((2,4-Dichlorophenyl)thio)-1H-imidazo[4,5-*c*]pyridin-4-amine (21d). Yield: 92%. 1H NMR (500 MHz, $CDCl_3$ /MeOH- d_4): δ 7.46–7.48 (m, 2H), 7.30 (d, $J = 8.5$ Hz, 1H), 7.02 (dd, $J = 8.5$, 2.2 Hz, 1H), 6.85 (d, $J = 6.4$ Hz, 1H). MS (ESI): m/z 310.8 $[M + H]^+$.

2-((3,5-Dichlorophenyl)thio)-1H-imidazo[4,5-*c*]pyridin-4-amine (21e). Yield: 71%. 1H NMR (500 MHz, MeOH- d_4): δ 7.47 (d, $J = 6.7$ Hz, 1H), 7.41–7.43 (m, 3H), 6.96 (d, $J = 6.7$ Hz, 1H). MS (ESI): m/z 310.8 $[M + H]^+$.

2-((6-Iodobenzo[d][1,3]dioxol-5-yl)thio)-1H-imidazo[4,5-*c*]pyridin-4-amine (21f). Yield: 78%. MS (ESI): m/z 412.8 $[M + H]^+$.

General Procedure for the Synthesis of 18d–f. To the appropriate intermediate (**21d–f**; 0.0477 mmol) in dry DMF (1.5 mL) were added Cs_2CO_3 (0.0572 mmol) and 1,3-dibromopropane (0.238 mmol), and the reaction mixture was stirred at rt for 2 h. The solvent was removed under reduced pressure and the crude product was purified by preparatory TLC [CH_2Cl_2 :MeOH–NH₃ (7 N), 20:1] to afford corresponding alkylated derivatives (confirmed by LC–MS). To these 3-bromopropyl alkylated intermediates (0.0175 mmol) in dry DMF was added isopropylamine (0.35 mmol), and the reaction mixture was stirred at rt for 24 h. Then, the solvent was removed under reduced pressure and the crude product was purified by preparatory TLC [CH_2Cl_2 :MeOH–NH₃ (7 N), 15:1] to afford the desired final products **18d–f**.

2-((2,4-Dichlorophenyl)thio)-1-(3-(isopropylamino)propyl)-1H-imidazo[4,5-*c*]pyridin-4-amine (18d). Yield: 35%. 1H NMR (500 MHz, $CDCl_3$): δ 7.86 (d, $J = 5.9$ Hz, 1H), 7.43 (d, $J = 2.2$ Hz, 1H), 7.13 (dd, $J = 8.5$, 2.2 Hz, 1H), 7.02 (d, $J = 8.6$ Hz, 1H), 6.75 (d, $J = 5.9$ Hz, 1H), 5.29 (br s, 2H), 4.25 (t, $J = 7.1$ Hz, 2H), 2.71 (m, 1H), 2.56 (t, $J = 6.8$ Hz, 2H), 1.88 (m, 2H), 1.02 (d, $J = 6.3$ Hz, 6H).

2-((3,5-Dichlorophenyl)thio)-1-(3-(isopropylamino)propyl)-1H-imidazo[4,5-*c*]pyridin-4-amine (18e). Yield: 39%. 1H NMR (500 MHz, $CDCl_3$): δ 7.88 (d, $J = 5.9$ Hz, 1H), 7.21–7.25 (m, 3H), 6.75 (d, $J = 5.9$ Hz, 1H), 5.26 (br s, 2H), 4.26 (t, $J = 7.1$ Hz, 2H), 2.71 (m, 1H), 2.56 (t, $J = 6.8$ Hz, 2H), 1.88 (m, 2H), 1.02 (d, $J = 6.2$ Hz, 6H). ^{13}C NMR (150 MHz, $CDCl_3$): δ 151.3, 142.7, 141.7, 140.8, 135.9, 135.7, 127.8, 127.5, 127.0, 97.6, 48.8, 44.0, 43.3, 30.5, 22.8. HRMS (ESI): m/z $[M + H]^+$ calcd for $C_{18}H_{22}N_5SCl_2$ 410.0973, found 410.0978.

2-((6-Iodobenzo[d][1,3]dioxol-5-yl)thio)-1-(3-(isopropylamino)propyl)-1H-imidazo[4,5-*c*]pyridin-4-amine (18f). Yield: 40%. 1H NMR (600 MHz, $CDCl_3$): δ 7.83 (d, $J = 5.9$ Hz, 1H), 7.26 (s, 1H), 6.77 (s, 1H), 6.73 (d, $J = 5.9$ Hz, 1H), 5.97 (s, 2H), 5.31 (br s, 2H), 4.23 (t, $J = 7.2$ Hz, 2H), 2.74–2.77 (m, 1H), 2.60 (t, $J = 6.9$ Hz, 2H), 1.90–1.93 (m, 2H), 1.06 (d, $J = 6.2$ Hz, 6H). ^{13}C NMR (150 MHz, $CDCl_3$): δ 151.2, 149.3, 148.6, 141.3, 140.9, 129.2, 127.4, 118.9, 111.2, 102.2, 97.5, 89.3, 48.9, 44.0, 43.3, 30.4, 22.8. HRMS (ESI): m/z $[M + H]^+$ calcd for $C_{19}H_{23}IN_5O_2S$ 512.0617, found 512.0628.

Reagents. Recombinant Hsp90 α (ADI-SPP-776), Hsp90 β (ADI-SPP-777), and Trap-1 (ADI-SPP-848) were purchased from Enzo Life Sciences. Canine Grp94 was generated as previously reported.⁵⁰

FP Measurements. The Hsp90 FP competition assays were performed on an Analyst GT instrument (Molecular Devices, Sunnyvale, CA) and carried out in black 96-well microplates (Corning # 3650) in a total volume of 100 μ L in each well. A stock of 10 μ M Cy3B-GM²¹ and PU-FITC3²² was prepared in DMSO and diluted with Felts buffer [20 mM Hepes (K), pH 7.3, 50 mM KCl, 2 mM DTT, 5 mM MgCl₂, 20 mM Na₂MoO₄, and 0.01% NP40 with 0.1 mg/mL BGG]. To each well was added the fluorescent dye labeled Hsp90 ligand (6 nM Cy3B-GM for Hsp90 α , Hsp90 β , and Grp94 and 3 nM PU-FITC3 for Trap-1), protein (10 nM Hsp90 α , 10 nM Hsp90 β , 10 nM Grp94, 30 nM Trap-1) and the tested inhibitor (initial stock in DMSO) in a final volume of 100 μ L of Felts buffer. Compounds were added in duplicate or triplicate wells. For each assay, background wells (buffer only), tracer controls (free, fluorescent dye labeled Hsp90 ligand only), and bound controls (fluorescent dye labeled Hsp90 ligand in the presence of protein) were included on each assay plate. The assay plate was incubated on a shaker at 4 °C for 24 h and the FP values (in mP) were measured. The fraction of fluorescent dye labeled

Hsp90 ligand bound to Hsp90 was correlated to the mP value and plotted against values of competitor concentrations. The inhibitor concentration at which 50% of bound fluorescent dye labeled Hsp90 ligand was displaced was obtained by fitting the data. For Cy3B-GM, an excitation filter at 530 nm and an emission filter at 580 nm were used with a dichroic mirror of 561 nm. For PU-FITC3, an excitation filter at 485 nm and an emission filter at 530 nm were used with a dichroic mirror of 505 nm. All experimental data were analyzed using SOFTmax Pro 4.3.1 and plotted using Prism 4.0 (Graphpad Software Inc., San Diego, CA).

Molecular Modeling. All computations were carried out on a HP workstation xw8200 with the Ubuntu 8.10 operating system using Maestro v8.5. Protein sequence and crystal structures were downloaded from NCBI and RCSB databases, respectively.

Ligand Preparation. All the compounds were constructed using the fragment dictionary of Maestro 8.5. The geometry of compounds was optimized using the MacroModel program v9.6 and the OLPS-AA force field.⁵¹ Ensuing ligands were further prepared using the Ligprep (v2.2) utility provided by Schrödinger LLC.

Docking. The X-ray crystal structure of PU-H54-bound Grp94 (PDB ID: 3O2F) was first aligned using a protein structure alignment tool and then optimized for subsequent grid generation and docking using the default parameters in Protein Preparation Wizard provided by Schrödinger LLC. Grids were then prepared using the Receptor Grid Generation tool in Glide 5.0.^{52,53} Next, the extraprecision (XP) Glide docking method was used to dock compounds flexibly into the ATP binding site of Grp94 according to the previously reported procedure.⁵⁴ Upon completion of each docking calculation, at most 100 poses per docking were run and at most 10 poses per ligand were allowed to be generated. Top-scored docking poses (orientation plus conformation) based on the Glide scoring (Gscore) function were analyzed. Docking accuracy was measured by resemblance of the lowest energy pose (binding conformation) predicted by the object scoring function Gscore with the experimental binding mode as determined by X-ray crystallography. Bound inhibitors PU-H54 (4) was removed from the Grp94 (PDB ID: 3O2F) binding site and redocked into the respective binding sites. Very good agreement was found between the localization of the inhibitor from docking and from the crystal structure with a RMSD of 0.04 Å (PDB ID: 3O2F) between the predicted conformation and the observed X-ray crystallographic conformation, validating the docking strategy.

Kinase Assays. For most assays, kinase-tagged T7 phage strains were grown in parallel in 24-well blocks in an *Escherichia coli* host derived from the BL21 strain. *E. coli* cells were grown to log-phase and infected with T7 phage from a frozen stock (multiplicity of infection = 0.4) and incubated with shaking at 32 °C until lysis (90–150 min). The lysates were centrifuged (6000g) and filtered (0.2 μm) to remove cell debris. The remaining kinases were produced in HEK-293 cells and subsequently tagged with DNA for qPCR detection. Streptavidin-coated magnetic beads were treated with biotinylated small molecule ligands for 30 min at room temperature to generate affinity resins for kinase assays. The liganded beads were blocked with excess biotin and washed with blocking buffer [SeaBlock (Pierce), 1% BSA, 0.05% Tween 20, 1 mM DTT] to remove unbound ligand and to reduce nonspecific phage binding. Binding reactions were assembled by combining kinases, liganded affinity beads, and test compounds in 1× binding buffer (20% SeaBlock, 0.17× PBS, 0.05% Tween 20, 6 mM DTT). Test compounds were prepared as 40× stocks in 100% DMSO and directly diluted into the assay. All reactions were performed in polypropylene 384-well plates in a final volume of 0.04 mL. The assay plates were incubated at room temperature with shaking for 1 h, and the affinity beads were washed with wash buffer (1× PBS, 0.05% Tween 20). The beads were then resuspended in elution buffer (1× PBS, 0.05% Tween 20, 0.5 μM nonbiotinylated affinity ligand) and incubated at room temperature with shaking for 30 min. The kinase concentration in the eluates was measured by qPCR.

Cell Lines. The HER2-overexpressing breast cancer cells SKBr3 were obtained from the American Type Culture Collection (ATCC). Cells were cultured routinely in McCoy's 5A supplemented with 10% FBS and 1% penicillin and streptomycin (Pen/Strep). C2C12 and

HEK293 cells were purchased from ATCC and cultured in DMEM in the presence of 10% FBS and 1% penicillin/streptomycin. RAW 264.7 cells was purchased from ATCC and cultured in DMEM with 2 mM L-glutamine, 10 mM HEPES, 1 mM sodium pyruvate, 10% low endotoxin FBS, and 1% Pen/Strep. When cultured, cells were incubated in the humidified cell incubators with CO₂ at 37 °C.

Immunoblotting. Cells were either treated with DMSO (vehicle) or indicated compounds for 24 h and lysed in RIPA buffer (50 mM Tris-HCl, pH 7.4, 150 mM NaCl, 0.5% sodium deoxycholate, and 0.5% NP40) supplemented with cocktail protease inhibitors (Roche) to produce whole-cell lysates. Protein concentrations were determined using the BCA kit (Pierce) according to the manufacturer's instructions. The protein lysates (5–50 μg) were electrophoretically resolved by SDS-PAGE, transferred onto nitrocellulose membranes, and probed with primary antibodies against HER2 (Zymed, 28004; 1:500), Hsp70 (Stressgen, SPA-810; 1:2500), cleaved PARP (Promega, G7341; 1:2500), and β-actin (Sigma, A1978; 1:3000). After washing off the excess antibodies, the membranes were incubated with the corresponding horseradish peroxidase (HRP)-conjugated secondary antibody. Blots were visualized by autoradiography using the Enhanced Chemiluminescence Detection System (GE Healthcare) according to the manufacturer's instructions. Films were scanned in Adobe Photoshop CS5, and quantitative densitometric analysis was performed using ImageJ (US National Institutes of Health).

Cell Viability Assessment. Cells were treated for 72 h with vehicle or inhibitors. Cell viability was assessed using CellTiter-Glo luminescent cell viability assay (Promega). The method determines the number of viable cells in culture based on quantification of the ATP present, which signals the presence of metabolically active cells. Drugs were added to quadruplicate wells.

C2C12 Differentiation and IGF-II Secretion Assay. C2C12 is an immortal line of mouse skeletal myoblasts originally derived from satellite cells from the thigh muscle of a 2-month-old female mouse donor. These cells differentiate well into myocytes under appropriate culture conditions. The cells were induced to differentiate by replacing the culture medium with DMEM supplemented with 2% horse serum and 1% penicillin/streptomycin (differentiation medium) for 36–48 h. Secreted IGF-II was quantified by using an IGF-II mouse ELISA kit (Abcam, AB100696) according to the manufacturer's instructions. Briefly, after shifting the culture medium to differentiation medium, C2C12 cells were treated for 24 h with the indicated compounds. Medium from each experimental condition was then transferred into ELISA plates coated with anti-IGF-II and incubated overnight at 4 °C. The bound IGF-II was detected with a biotinylated anti-IGF-II antibody provided in the kit. After the sequential incubation with HRP-conjugated streptavidin, TMB one-step substrate reagent, and the stop solution, the absorbance was measured at 450 nm. The secreted IGF-II was quantified against a standard curve generated with recombinant IGF-II provided by the kit.

TLR9 Assay. HEK 293T cells were transfected with pUNO-hTLR9-HA (InvivoGen) using X-tremgene HP (Roche) according to the manufacturer's instructions. At 24 h after transfection, cells were split onto cell culture chamber slides (Lab-Tek). Cells were then treated for 24 h with compounds at varying concentrations. After treatment, cells were fixed for 20 min in 4% paraformaldehyde in PBS, permeabilized with 0.1% Triton X-100 in PBS for 10 min, and blocked with 3% BSA in PBS for 30 min, followed by staining for 1 h with anti-HA (Abcam, ab9110; 1:250) or a normal rabbit IgG (Abcam, ab37415; 1:250). Cells were washed with PBS, stained with an anti-rabbit-Cy3 antibody (Invitrogen, A10520; 1:400), and finally mounted in the dark at 4 °C with with one drop of Prolong Gold Antifade reagent (with DAPI, Life Technologies, P36935). Cells were visualized under a confocal microscope (Leica Upright Confocal SP5). Fluorescence intensity was quantified using MetaMorph Microscopy Automation and Image Analysis Software (Molecular Devices Inc.) and normalized to the cell number.

TNFα ELISA. Raw264.7 cells were stimulated with 10 ng/mL LPS or 2.5 μM ODN1585 (G*G*G* GTC AAC GTT GAG G*G*G* G*G), followed by the 18 h treatments with the indicated inhibitors.

The mouse TNF α ELISA MAX Set (BioLegend) was used to quantify the TNF α according to the manufacturer's instructions.

Animal Studies. Four- to 6-week-old *nu/nu* athymic female mice were obtained from Harlan Laboratories. Experiments were carried out under an Institutional Animal Care and Use Committee approved protocol, and institutional guidelines for the proper and humane use of animals in research were followed. MDA-MB-468 cells (1×10^7) were sc implanted in the right flank of mice using a 20-gauge needle and allowed to grow. All mice received Augmentin (amoxicillin/clavulanate potassium; SmithKline Beecham) in their drinking water while on therapy. Mice were sacrificed by CO₂ euthanasia.

Pharmacodynamic (PD) and Pharmacokinetic (PK) Studies. 18c (75 or 150 mg/kg, ip) was administered to mice ($n = 4$) bearing breast tumors, and mice were sacrificed at 2 and 24 h postadministration. Drug levels in tissues and plasma were determined by LC-MS/MS. Compound 18c was injected as a single dose intravenously or orally at 10 mg/kg to B6D2F1 mice ($n = 2$ male mice per experimental point, 20 mice total). The agent was formulated in 30% captisol, 5 mM citrate buffer at pH 4.2. Drug levels in plasma were determined by LC-MS/MS.

■ ASSOCIATED CONTENT

🔍 Supporting Information

Experimental details for the synthesis of 18g and Figures S1–S4. This material is available free of charge via the Internet at <http://pubs.acs.org>.

■ AUTHOR INFORMATION

✉ Corresponding Authors

*T.T.: phone, 646-888-3180. e-mail, taldonet@mskcc.org.

*G.C.: phone, 646-888-2235. e-mail, chiosisg@mskcc.org.

👤 Author Contributions

H.J.P., P.D.P., S.O.O., P.Y., W.S., and M.R.P. contributed equally.

📌 Notes

The authors declare no competing financial interest.

■ ACKNOWLEDGMENTS

H.J.P. is funded by Susan G. Komen, Award # PDF14301695, S.O.O. is supported by PF-14-154-01-CDD from the American Cancer Society, P.Y. is supported by AACI Translational Cancer Research Fellowship. G.C. is funded by the Leukemia and Lymphoma Society, Breast Cancer Research Fund, U01 AG032969-01A1, R21 AI090501, R01 CA172546, and R01 CA155226. P.D.P. and R.A.S. are supported by funds and resources from St. John's University. Z.L. is funded by R01 AI070603 and R01 AI077283, C.L. and J.B. by R03 AI097671 and R01 AI076588, and D.G. by R01 CA095130.

■ ABBREVIATIONS USED

Hsp90, heat shock protein 90; Grp94, glucose regulated protein 94; ER, endoplasmic reticulum; Trap-1, tumor necrosis factor receptor-associated protein-1; Abs, antibodies; TLRs, toll-like receptors; IgG, immunoglobulin; RA, rheumatoid arthritis; HUVECs, human umbilical vein endothelial cells

■ REFERENCES

(1) Sorger, P. K.; Pelham, H. R. The glucose-regulated protein Grp94 is related to heat shock protein Hsp90. *J. Mol. Biol.* **1987**, *194*, 341–344.
(2) Marzec, M.; Eletto, D.; Argon, Y. GRP94: An HSP90-like protein specialized for protein folding and quality control in the endoplasmic reticulum. *Biochim. Biophys. Acta* **2012**, *1823*, 774–787.
(3) Whitesell, L.; Lindquist, S. L. Hsp90 and the chaperoning of cancer. *Nat. Rev. Cancer* **2005**, *5*, 761–772.

(4) Altieri, D. C.; Stein, G. S.; Lian, J. B.; Languino, L. R. TRAP-1, the mitochondrial Hsp90. *Biochim. Biophys. Acta* **2012**, *1823*, 767–773.

(5) Kang, B. H.; Plescia, J.; Dohi, T.; Rosa, J.; Doxsey, S. J.; Altieri, D. C. Regulation of tumor cell mitochondrial homeostasis by an organelle-specific Hsp90 chaperone network. *Cell* **2007**, *131*, 257–270.

(6) Costantino, E.; Maddalena, F.; Calise, S.; Piscazzi, A.; Tirino, V.; Fersini, A.; Ambrosi, A.; Neri, V.; Esposito, F.; Landriscina, M. TRAP1, a novel mitochondrial chaperone responsible for multi-drug resistance and protection from apoptosis in human colorectal carcinoma cells. *Cancer Lett.* **2009**, *279*, 39–46.

(7) Lee, A. S. Glucose-regulated proteins in cancer: Molecular mechanisms and therapeutic potential. *Nat. Rev. Cancer* **2014**, *14*, 263–276.

(8) Yang, Y.; Liu, B.; Dai, J.; Srivastava, P. K.; Zammit, D. J.; Lefrançois, L.; Li, Z. Heat shock protein gp96 is a master chaperone for toll-like receptors and is important in the innate function of macrophages. *Immunity* **2007**, *26*, 215–226.

(9) Hua, Y.; White-Gilbertson, S.; Kellner, J.; Rachidi, S.; Usmani, S. Z.; Chiosis, G.; Depinho, R.; Li, Z.; Liu, B. Molecular chaperone gp96 is a novel therapeutic target of multiple myeloma. *Clin. Cancer Res.* **2013**, *19*, 6242–6251.

(10) Patel, P. D.; Yan, P.; Seidler, P. M.; Patel, H. J.; Sun, W.; Yang, C.; Que, N. S.; Taldone, T.; Finotti, P.; Stephani, R. A.; Gewirth, D. T.; Chiosis, G. Paralog-selective Hsp90 inhibitors define tumor-specific regulation of HER2. *Nat. Chem. Biol.* **2013**, *9*, 677–684.

(11) Soldano, K. L.; Jivan, A.; Nicchitta, C. V.; Gewirth, D. T. Structure of the N-terminal domain of GRP94. *J. Biol. Chem.* **2003**, *279*, 48330–48338.

(12) Rosser, M. F.; Nicchitta, C. V. Ligand interactions in the adenine nucleotide-binding domain of the Hsp90 chaperone, GRP94. I. Evidence for allosteric regulation of ligand binding. *J. Biol. Chem.* **2000**, *275*, 22798–22805.

(13) Immormino, R. M.; Dollins, D. E.; Shaffer, P. L.; Soldano, K. L.; Walker, M. A.; Gewirth, D. T. Ligand-induced conformational shift in the N-terminal domain of GRP94, an Hsp90 chaperone. *J. Biol. Chem.* **2004**, *279*, 46162–46171.

(14) Immormino, R. M.; Metzger, L. E.; Reardon, P. N.; Dollins, D. E.; Blagg, B. S.; Gewirth, D. T. Different poses for ligand and chaperone in inhibitor-bound Hsp90 and GRP94: Implications for paralog-specific drug design. *J. Mol. Biol.* **2009**, *388*, 1033–1042.

(15) Cristalli, G.; Lambertucci, C.; Taffi, S.; Vittori, S.; Volpini, R. Medicinal chemistry of adenosine A2A receptor agonists. *Curr. Top. Med. Chem.* **2003**, *3*, 387–401.

(16) Clevenger, R. C.; Blagg, B. S. Design, synthesis, and evaluation of a radicicol and geldanamycin chimera, radamide. *Org. Lett.* **2004**, *6*, 4459–4462.

(17) Duerfeldt, A. S.; Peterson, L. B.; Maynard, J. C.; Ng, C. L.; Eletto, D.; Ostrovsky, O.; Shinogle, H. E.; Moore, D. S.; Argon, Y.; Nicchitta, C. V.; Blagg, B. S. Development of a Grp94 inhibitor. *J. Am. Chem. Soc.* **2012**, *134*, 9796–9804.

(18) Stothert, A. R.; Suntharalingam, A.; Huard, D. J.; Fontaine, S. N.; Crowley, V. M.; Mishra, S.; Blagg, B. S.; Lieberman, R. L.; Dickey, C. A. Exploiting the interaction between Grp94 and aggregated myocilin to treat glaucoma. *Hum. Mol. Genet.* **2014**, *23*, 6470–6480.

(19) Bao, R.; Lai, C. J.; Qu, H.; Wang, D.; Yin, L.; Zifcak, B.; Atoyian, R.; Wang, J.; Samson, M.; Forrester, J.; DellaRocca, S.; Xu, G. X.; Tao, X.; Zhai, H. X.; Cai, X.; Qian, C. CUDC-305, a novel synthetic HSP90 inhibitor with unique pharmacologic properties for cancer therapy. *Clin. Cancer Res.* **2009**, *15*, 4046–4057.

(20) Cai, X.; Qian, C.; Zhai, H. Preparation of imidazo[4,5-c]pyridine derivatives as HSP90 inhibitors. Patent WO2008115719A1, 2008.

(21) Moullick, K.; Clement, C. C.; Aguirre, J.; Kim, J.; Kang, Y.; Felts, S.; Chiosis, G. Synthesis of a red-shifted fluorescence polarization probe for Hsp90. *Bioorg. Med. Chem. Lett.* **2006**, *16*, 4515–4518.

(22) Taldone, T.; Patel, P. D.; Patel, M.; Patel, H. J.; Evans, C. E.; Rodina, A.; Ochiana, S.; Shah, S. K.; Uddin, M.; Gewirth, D.; Chiosis, G. Experimental and structural testing module to analyze paralogue-

specificity and affinity in the Hsp90 inhibitors series. *J. Med. Chem.* **2013**, *56*, 6803–6818.

(23) He, H.; Llauger, L.; Rosen, N.; Chiosis, G. General method for the synthesis of 8-arylsulfanyl adenine derivatives. *J. Org. Chem.* **2004**, *69*, 3230–3232.

(24) Llauger, L.; He, H.; Kim, J.; Aguirre, J.; Rosen, N.; Peters, U.; Davies, P.; Chiosis, G. Evaluation of 8-arylsulfanyl, 8-arylsulfoxyl, and 8-arylsulfonyl adenine derivatives as inhibitors of the heat shock protein 90. *J. Med. Chem.* **2005**, *48*, 2892–2905.

(25) Biamonte, M. A.; Shi, J.; Hong, K.; Hurst, D. C.; Zhang, L.; Fan, J.; Busch, D. J.; Karjian, P. L.; Maldonado, A. A.; Sensintaffar, J. L.; Yang, Y. C.; Kamal, A.; Lough, R. E.; Lundgren, K.; Burrows, F. J.; Timony, G. A.; Boehm, M. F.; Kasibhatla, S. R. Orally active purine-based inhibitors of the heat shock protein 90. *J. Med. Chem.* **2006**, *49*, 817–828.

(26) Taldone, T.; Patel, P. D.; Patel, H. J.; Chiosis, G. About the reaction of aryl fluorides with sodium sulfide: Investigation into the selectivity of substitution of fluorobenzonitriles to yield mercapto-benzonitriles via SNAr displacement of fluorine. *Tetrahedron Lett.* **2012**, *53*, 2548–2551.

(27) Tao, H.; Kang, Y.; Taldone, T.; Chiosis, G. Microwave-assisted one step synthesis of 8-arylmethyl-9H-purin-6-amines. *Bioorg. Med. Chem. Lett.* **2009**, *19*, 415–417.

(28) He, H.; Zatorska, D.; Kim, J.; Aguirre, J.; Llauger, L.; She, Y.; Wu, N.; Immormino, R. M.; Gewirth, D. T.; Chiosis, G. Identification of potent water soluble purine-scaffold inhibitors of the heat shock protein 90. *J. Med. Chem.* **2006**, *49*, 381–390.

(29) Chiosis, G.; Lucas, B.; Shtil, A.; Huezo, H.; Rosen, N. Development of a purine-scaffold novel class of Hsp90 binders that inhibit the proliferation of cancer cells and induce the degradation of Her2 tyrosine kinase. *Bioorg. Med. Chem.* **2002**, *10*, 3555–3564.

(30) Immormino, R. M.; Kang, Y.; Chiosis, G.; Gewirth, D. T. Structural and quantum chemical studies of 8-aryl-sulfanyl adenine class Hsp90 inhibitors. *J. Med. Chem.* **2006**, *49*, 4953–4960.

(31) Fabian, M. A.; Biggs, W. H., 3rd; Treiber, D. K.; Atteridge, C. E.; Azimioara, M. D.; Benedetti, M. G.; Carter, T. A.; Ciceri, P.; Edeen, P. T.; Floyd, M.; Ford, J. M.; Galvin, M.; Gerlach, J. L.; Grotzfeld, R. M.; Herrgard, S.; Insko, D. E.; Insko, M. A.; Lai, A. G.; Lélías, J. M.; Mehta, S. A.; Milanov, Z. V.; Velasco, A. M.; Wodicka, L. M.; Patel, H. K.; Zarrinkar, P. P.; Lockhart, D. J. A small molecule-kinase interaction map for clinical kinase inhibitors. *Nat. Biotechnol.* **2005**, *23*, 329–336.

(32) Taldone, T.; Ochiana, S.; Patel, P. D.; Chiosis, G. Selective targeting of the stress chaperome as a therapeutic strategy. *Trends Pharmacol. Sci.* **2014**, *35*, 592–603.

(33) Medzhitov, R. Toll-like receptors and innate immunity. *Nat. Rev. Immunol.* **2001**, *1*, 135–145.

(34) Brooks, J. C.; Sun, W.; Chiosis, G.; Leifer, C. A. Heat shock protein gp96 regulates toll-like receptor 9 proteolytic processing and conformational stability. *Biochem. Biophys. Res. Commun.* **2012**, *421*, 780–784.

(35) Ostrovsky, O.; Ahmed, N. T.; Argon, Y. The chaperone activity of GRP94 towards of insulin-like growth factor II is necessary for the stress response to serum deprivation. *Mol. Biol. Cell* **2009**, *20*, 1855–1864.

(36) Neckers, L. Heat shock protein 90: The cancer chaperone. *J. Biosci.* **2007**, *32*, 517–530.

(37) Supko, J. G.; Hickman, R. L.; Grever, M. R.; Malspeis, L. Preclinical pharmacologic evaluation of geldanamycin as an antitumor agent. *Cancer Chemother. Pharmacol.* **1995**, *36*, 305–315.

(38) Neckers, L. Chaperoning oncogenes: Hsp90 as a target of geldanamycin. *Handb. Exp. Pharmacol.* **2006**, 259–277.

(39) Jhaveri, K.; Ochiana, S. O.; Dunphy, M. P.; Gerecitano, J. F.; Corben, A. D.; Peter, R. I.; Janjigian, Y. Y.; Gomes-DaGama, E. M.; Koren, J., 3rd; Modi, S.; Chiosis, G. Heat shock protein 90 inhibitors in the treatment of cancer: Current status and future directions. *Expert Opin. Invest. Drugs* **2014**, *23*, 611–628.

(40) Patel, H. J.; Modi, S.; Chiosis, G.; Taldone, T. Advances in the discovery and development of heat-shock protein 90 inhibitors for cancer treatment. *Expert Opin. Drug Discovery* **2011**, *6*, 559–587.

(41) Matts, R. L.; Brandt, G. E.; Lu, Y.; Dixit, A.; Mollapour, M.; Wang, S.; Donnelly, A. C.; Neckers, L.; Verkhivker, G.; Blagg, B. S. A systematic protocol for the characterization of Hsp90 modulators. *Bioorg. Med. Chem.* **2011**, *19*, 684–692.

(42) Moullick, K.; Ahn, J. H.; Zong, H.; Rodina, A.; Cerchietti, L.; Gomes DaGama, E. M.; Caldas-Lopes, E.; Beebe, K.; Perna, F.; Hatzi, K.; Vu, L. P.; Zhao, X.; Zatorska, D.; Taldone, T.; Smith-Jones, P.; Alpaugh, M.; Gross, S. S.; Pillarsetty, N.; Ku, T.; Lewis, J. S.; Larson, S. M.; Levine, R.; Erdjument-Bromage, H.; Guzman, M. L.; Nimer, S. D.; Melnick, A.; Neckers, L.; Chiosis, G. Affinity-based proteomics reveal cancer-specific networks coordinated by Hsp90. *Nat. Chem. Biol.* **2011**, *7*, 818–826.

(43) Beebe, K.; Mollapour, M.; Scroggins, B.; Prodromou, C.; Xu, W.; Tokita, M.; Taldone, T.; Pullen, L.; Zierer, B. K.; Lee, M. J.; Trepel, J.; Buchner, J.; Bolon, D.; Chiosis, G.; Neckers, L. Posttranslational modification and conformational state of heat shock protein 90 differentially affect binding of chemically diverse small molecule inhibitors. *Oncotarget* **2013**, *4*, 1065–1074.

(44) Mollapour, M.; Bourboulia, D.; Beebe, K.; Woodford, M. R.; Polier, S.; Hoang, A.; Chelluri, R.; Li, Y.; Guo, A.; Lee, M. J.; Fotooh-Abadi, E.; Khan, S.; Prince, T.; Miyajima, N.; Yoshida, S.; Tsutsumi, S.; Xu, W.; Panaretou, B.; Stetler-Stevenson, W. G.; Bratslavsky, G.; Trepel, J. B.; Prodromou, C.; Neckers, L. Asymmetric Hsp90 N domain SUMOylation recruits Aha1 and ATP-competitive inhibitors. *Mol. Cell* **2014**, *53*, 317–329.

(45) Kamal, A.; Thao, L.; Sensintaffar, J.; Zhang, L.; Boehm, M. F.; Fritz, L. C.; Burrows, F. J. A high-affinity conformation of Hsp90 confers tumour selectivity on Hsp90 inhibitors. *Nature* **2003**, *425*, 407–410.

(46) Cerchietti, L. C.; Lopes, E. C.; Yang, S. N.; Hatzi, K.; Bunting, K. L.; Tsikitas, L. A.; Mallik, A.; Robles, A. I.; Walling, J.; Varticovski, L.; Shaknovich, R.; Bhalla, K. N.; Chiosis, G.; Melnick, A. A purine scaffold Hsp90 inhibitor destabilizes BCL-6 and has specific antitumor activity in BCL-6-dependent B cell lymphomas. *Nat. Med.* **2009**, *15*, 1369–1376.

(47) Breinig, M.; Caldas-Lopes, E. M.; Goepfert, B.; Malz, M.; Bergmann, F.; Rieker, R.; Schirmacher, P.; Chiosis, G.; Kern, M. A. Targeting the heat shock protein Hsp90 with non-quinone inhibitors: A novel chemotherapeutic approach in human hepatocellular carcinoma. *Hepatology* **2009**, *50*, 102–112.

(48) Caldas-Lopes, E.; Cerchietti, L.; Ahn, J. H.; Clement, C. C.; Robles, A. I.; Rodina, A.; Moullick, K.; Taldone, T.; Gozman, A.; Guo, Y.; Wu, N.; de Stanchina, E.; White, J.; Gross, S. S.; Ma, Y.; Varticovski, L.; Melnick, A.; Chiosis, G. Hsp90 inhibitor PU-H71, a multimodal inhibitor of malignancy, induces complete responses in triple-negative breast cancer models. *Proc. Natl. Acad. Sci. U. S. A.* **2009**, *106*, 8368–8373.

(49) Rodina, A.; Vilenchik, M.; Moullick, K.; Aguirre, J.; Kim, J.; Chiang, A.; Litz, J.; Clement, C. C.; Kang, Y.; She, Y.; Wu, N.; Felts, S.; Wipf, P.; Massague, J.; Jiang, X.; Brodsky, J. L.; Krystal, G. W.; Chiosis, G. Selective compounds define Hsp90 as a major inhibitor of apoptosis in small cell lung cancer. *Nat. Chem. Biol.* **2007**, *3*, 498–507.

(50) Dollins, D. E.; Immormino, R. M.; Gewirth, D. T. Structure of unliganded GRP94, the endoplasmic reticulum Hsp90. Basis for nucleotide-induced conformational change. *J. Biol. Chem.* **2005**, *280*, 30438–30447.

(51) Jorgensen, W. L.; Maxwell, D.; Tirado-Rives, J. Development and testing of the OPLS-All Atom force field on conformational energetics and properties of organic liquids. *J. Am. Chem. Soc.* **1996**, *118*, 11225–11236.

(52) Friesner, R. A.; Banks, J. L.; Murphy, R. B.; Halgren, T. A.; Klicic, J. J.; Mainz, D. T.; Repasky, M. P.; Knoll, E. H.; Shelley, M.; Perry, J. K.; Shaw, D. E.; Francis, P.; Shenkin, P. S. Glide: A new approach for rapid, accurate docking and scoring. 1. Method and assessment of docking accuracy. *J. Med. Chem.* **2004**, *47*, 1739–1749.

(53) Halgren, T. A.; Murphy, R. B.; Friesner, R. A.; Beard, H. S.; Frye, L. L.; Pollard, W. T.; Banks, J. L. Glide: A new approach for rapid, accurate docking and scoring. 2. Enrichment factors in database screening. *J. Med. Chem.* **2004**, *47*, 1750–1759.

(54) Patel, P. D.; Patel, M. R.; Kaushik-Basu, N.; Talele, T. T. 3D QSAR and molecular docking studies of benzimidazole derivatives as hepatitis C virus NSSB polymerase inhibitors. *J. Chem. Inf. Model.* **2008**, *48*, 42–55.